Tfap2b specifies an embryonic melanocyte stem cell population that retains adult multi-fate potential

Alessandro Brombin[1,2], Daniel J. Simpson[1], Jana Travnickova[1,2], Hannah R. Brunsdon[1,2], Zhiqiang Zeng[1,2], Yuting Lu[1,2], Tamir Chandra[1, 3], E. Elizabeth Patton[1,2,3, 4]

1. MRC Human Genetics Unit, Institute of Genetics and Cancer, University of Edinburgh, Western General Hospital Campus, EH4 2XU, Edinburgh, United Kingdom.

2. CRUK Edinburgh Centre, Institute of Genetics and Cancer, University of Edinburgh, Western General Hospital Campus, EH4 2XU, Edinburgh, United Kingdom.

3. Corresponding authors: tamir.chandra@ed.ac.uk, e.patton@ed.ac.uk

4. Lead contact

Summary

Melanocytes, our pigment producing cells, originate from neural crest-derived progenitors during embryogenesis and from multiple stem cell niches in adult tissues. Although pigmentation traits are known risk-factors for melanoma, we lack lineage markers with which to identify melanocyte stem cell populations and study their function. Here, by combining live-imaging, scRNA-seq and chemical-genetics in zebrafish, we identify the transcription factor Tfap2b as a functional marker for the melanocyte stem cell (MSC) population that resides at the dorsal root ganglia site. Tfap2b is required for only a few late-stage embryonic melanocytes, and instead is essential for MSC-dependent melanocyte regeneration. Our lineage-tracing data reveal that *tfap2b*-expressing MSCs have multi-fate potential, and are the cell-of-origin for a discrete number of embryonic melanocytes, large patches of adult melanocytes, and two other pigment cell types; iridophores and xanthophores. Hence, Tfap2b confers MSC identity, and thereby distinguishes MSCs from other neural crest and pigment cell lineages.

Highlights

- scRNA sequencing reveals pigment cell progenitors with multi-fate transcriptomes
- *tfap2b* expression marks an ErbB-dependent cell progenitor at the stem cell niche
- *tfap2b* is required for melanocyte regeneration from the melanocyte stem cell lineage
- Lineage tracing reveals *tfap2b* cells have multi-fate potential for adult pigment cells

Keywords

Melanocyte stem cells, pigment stem cells, neural crest cells, *tfap2b*, ErbB signaling, melanocyte lineage, scRNA-seq, lineage tracing, chemical genetics, zebrafish

Introduction

Melanocytes produce black-brown pigment that give color and pattern to the animal kingdom, and protect from harmful UV-irradiation (Mort et al., 2015; Nguyen and Fisher 2019). How melanocytes develop in embryogenesis and maintain a regenerative melanocyte population in adulthood is central to our understanding of pigmentation and pattern formation through evolution, as well as in human disease (Baxter and Pavan, 2013; Irion and Nusslein-Volhard, 2019; Kelsh and Barsh, 2011; Kinsler and Larue, 2018; Nusslein-Volhard and Singh, 2017; Parichy and Spiewak, 2015). In melanoma, a deadly cancer of the melanocyte, neural crest and melanocyte developmental mechanisms become reactivated in pathological processes driving melanoma initiation, metastasis, survival and drug resistance (Diener and Sommer, 2020; Kaufman et al., 2016; Konieczkowski et al., 2014; Marie et al., 2020; Rambow et al., 2018; Shakhova et al., 2012; Travnickova et al., 2019; Varum et al., 2019; White et al., 2011). Therefore, mechanisms that underpin neural crest (NC) and melanocyte developmental dysregulation and heterogeneity in cancer provide a rich source of drug targets for the next generation of melanoma therapies (Patton et al., 2021).

Zebrafish are uniquely amenable to advanced imaging of neural crest and pigment cell lineage pathways *in vivo*, and have emerged as a powerful model system to study the melanocyte developmental lineage in pattern formation and in melanoma (Kelsh et al., 1996; Owen et al., 2020; Travnickova and Patton, 2021). In zebrafish, embryonic trunk melanocytes are directly derived from the neural crest, but a rare melanocyte subset present in the lateral stripe originates from melanocyte stem cells (MSCs), a postembryonic progenitor population dependent on ErbB-kinase signaling (the epidermal growth factor family of receptor tyrosine kinases) (Irion et al., 2016; Mort et al., 2015; Parichy and Spiewak, 2015). MSCs are essential for replenishing melanocytes following regeneration or during adult growth, and ablation or genetic loss of MSCs leads to large patches of skin devoid of pigment cells in the adult fish (Budi et al., 2008; Hultman

and Johnson, 2010; Krauss et al., 2014; O'Reilly-Pol and Johnson, 2009; Taylor et al., 2011; Tryon et al., 2011; Zhou et al., 2012). Imaging analysis in zebrafish over time shows that MSCs reside in a niche at the site of the dorsal root ganglia (DRG) and give rise to progenitors that migrate along nerves to the epidermis, where they differentiate into pigmented melanocytes (Budi et al., 2011; Dooley et al., 2013; Singh et al., 2016; Singh et al., 2014).

In mammals, multiple melanocyte stem cell populations have been identified at distinct anatomical locations. In the skin, a melanocyte stem cell (McSC) population residing in the hair follicle is a reservoir for hair and skin melanocytes during the hair cycle and for re-pigmentation in vitiligo, and is a cellular origin of melanoma (Lee and Fisher, 2014; Moon et al., 2017; Sun et al., 2019). On hairless skin, such as the palm or sole, the sweat gland serves as a niche for melanocyte – melanoma precursors (Okamoto et al., 2014). In the dermis, a multi-potent stem cell that expresses neural-crest markers NGFRp75 and Nestin is a source of extrafollicular epidermal melanocytes, as well as mesenchymal and neuronal lineages (Li et al., 2010; Zabierowski et al., 2011). These cell populations may be similar to the multi-potent NC-derived Schwann-cell precursor (SCP) population in chick and mouse that gives rise to melanocytes (Furlan and Adameyko, 2018). SCPs migrate ventrally from the neural crest to the DRG, and then reside along the growing nerve, representing a niche for various cell types, including melanocytes (Adameyko et al., 2009; Diener and Sommer, 2020; Ernfors, 2010). Zebrafish do not have hair, but the zebrafish MSC anatomical niche site suggests that zebrafish MSCs are functionally analogous to the SCP population found in birds and mammals (Budi et al., 2011; Dooley et al., 2013).

In zebrafish, Sox-10 lineage tracing proposed a cell population called MIX cells, a neural crest cell subpopulation that is multi-potent for all three pigment cell types - black-brown melanocytes, silver iridophores and yellow xanthophores - and that gives rise to neurons and glia (Singh et al., 2016). MIX cells persist beyond embryonic and larval stages and are present into adulthood, where they are the source of almost all adult melanocytes and pattern the adult fish (Singh et al.,

2016). Through this body of work, it's clear that pigment stem cells emerge from the neural crest in zebrafish development, but because there are no cell specific markers with which to directly identify pigment stem cells *in vivo,* how these become specified or are related to the MSC is unknown.

Here, through the use of single cell RNA sequencing (scRNA-seq), imaging and lineage tracing approaches, we discover that the transcription factor *tfap2b* marks an ErbB-dependent multipotent cell population. Although a mutation in its gene paralog *tfap2a* is associated with premature hair greying in humans (Praetorius et al., 2013) and results in pigmentation defects in mice and zebrafish (Seberg et al., 2017), the role of *tfap2b* in melanocyte biology is entirely unexplored. In melanoma, *TFAP2B* marks a critical node in residual disease cell states (Rambow et al., 2018), although it's precise function is yet to be defined. We show that the *tfap2b*-marked cell population resides in the MSC niche and is a progenitor for all three pigment cell lineages. Our data support the conclusion that *tfap2b*-expressing cells are a subset within the MIX cell population that is responsible for generating melanocytes and other pigment cell lineages that emerge from the MSC lineage in adult zebrafish.

Results

MSCs maintain a neural crest identity at the niche

To visualize MSCs as they migrate into the DRG-niche site, we performed live imaging of zebrafish embryos. To this end, we used the transgenic reporter lines *Tg(mitfa:GFP*), that marks melanoblasts, and *Tg(nbt:dsRed*)*,* that marks the neural tube and peripheral nerves (Dooley et al., 2013). Prior to melanisation, during the first 22-27 hours of development, we observed a GFP+ subpopulation that traversed the MSC niche and migrated along peripheral nerves to the skin (**Figure 1A, B**). We consider these to be melanocytes that develop directly from the NC and use

nerves to migrate to the anatomical location where they generate the embryonic stripes. Subsequently, we observed a distinct, smaller subpopulation of round melanoblasts that was maintained at the niche and a population of stationary columnal cells that coated the nerves (**Figure 1A, C**). These cell populations have previously been described as MSCs and progenitors (Budi et al., 2011; Dooley et al., 2013; Johansson et al., 2020; Kelsh and Barsh, 2011; Singh et al., 2016; Singh et al., 2014). We confirmed that the small, round *mitfa*+ cells were MSCs through treatment with an ErbB inhibitor, which eliminated this population at the niche site, as well as nerve-associated progenitors (**Figure 1D-E**) (Budi et al., 2008, 2011; Dooley et al., 2013; Hultman et al., 2009).

Tg(mitfa:GFP) is expressed by MSCs, but it's neither an exclusive MSC marker nor does *mitfa* mutation or knockdown prevent acquisition of MSC identity or establishment at the DRG-niche (Budi et al., 2011; Dooley et al., 2013; Johnson et al., 2011), indicating that unknown mechanisms confer MSC identity from the neural crest. To resolve such mechanisms and identify specific MSC markers, we generated a *Tg(mitfa:GFP; crestin:mCherry)* double transgenic line that enabled visualization of both the *mitfa*-expressing melanocyte lineage (GFP+) as well as its origin in the neural crest lineage (mCherry+) (Kaufman et al., 2016) during MSC establishment. In the double transgenic line, we observed newly established MSCs that retained neural crest expression (GFP+ mCherry+) and cell columns along the peripheral nerves (**Figure 1F**), however, the expression levels for both GFP and mCherry fluorescence was heterogenous for both cell populations (**Figure 1F-G**). By 48hpf GFP+ mCherry+ fluorescence was restricted specifically to the MSCs, while differentiating melanoblasts maintained GFP+ fluorescence (**Figure 1G**). In the MSCs, expression of both transgenes was maintained through organogenesis before eventually subsiding by 120 hpf (**Figure 1G**). Thus, unlike differentiating melanoblasts found in the skin, the MSC subpopulation maintains a neural crest identity during the stem cell establishment and specification phase.

scRNA-seq identifies six distinct neural crest-pigment cell lineage populations

To identify a molecular signature specific for MSCs we needed to first understand how pigment cell populations arise from NC. To this end, we performed droplet-based scRNA-seq on GFP+ and/or mCherry+ cells sorted from the *Tg(mitfa:GFP; crestin:mCherry)* transgenic line using the 10x Chromium system (10x Genomics; **Figure 2A, Figure S1A;** see STAR methods); sequencing 1022 cellular transcriptomes, 996 of which passed our quality control (**Figure S1B-J**). When we visualised the data into a two-dimensional space, by applying the Louvain clustering algorithm (Butler et al., 2018) and the Uniform Manifold Approximation and Projection (UMAP; (McInnes et al., 2018) (**Figure 2B**), we found that expressed genes and number of Unique Molecular Identifiers were uniformly distributed across the cell populations (**Figure S2A-B, Table S1**).

To assign cluster identities, we employed a combination of known markers and projections to previously published datasets (Farnsworth et al., 2020; Kiselev et al., 2018; Saunders et al., 2019; Wagner et al., 2018) (**Figure S2C-F, Table S2**). We identified two proliferative neural crest cell (NCC) populations expressing classical neural crest markers, one of which was characterised by the almost exclusive expression of the bHLH transcription factor and EMT gene *twist1a* (and other *twist* genes) and the second by expression of *foxd3*, a known Wnt-regulated NC gene (**Figure 2B-D, Table S2**). In addition, we identified four distinct pigment progenitor cell clusters that expressed a combination of different chromatophore markers. Overall, these aligned with the hypothesised cell populations described through *sox10*+ lineage tracing experiments (Singh et al., 2016); namely, MIX progenitors, MX progenitors, MI progenitors and Melanoblasts (with M, I, and X standing for melanocyte, iridophore and xanthophore markers) (**Figure 2B-D**). The MIX progenitors cluster expressed NCC genes, *id* genes, and a combination of chromatophore markers, including melanocyte (*mitfa*, *dct* and *tyrp1b*), xanthoblast (*aox5*) and iridophore (*pnp4a*) markers. Thus, the MIX progenitor cluster represents a neural crest cell type that has the potential

to give rise to all pigment cell lineages but is not yet restricted towards a specific chromatophore type. We were intrigued to see that cells belonging to this cluster expressed less than half of the genes overall. This molecular phenotype is congruent with a stem cell identity, as self-renewing hematopoietic stem cells (HSCs), at the top of the differentiation hierarchy, express the lowest number of genes and total mRNA, with total mRNA expression gradually increasing in differentiated cells (Nestorowa et al., 2016) (**Figure S2B**). Cells in the immediately adjacent clusters expressed relatively high levels of melanoblast markers concomitant with markers for different chromatophores: MX progenitors expressed *mitfa* and *aox5* and MI progenitors expressed *mitfa* and *pnp4a* (**Figure 2C-D**). Melanoblasts were very similar to MI progenitors in gene expression profile but had higher expression level of melanocyte differentiation genes. We did not find evidence of IX cells in our experiment.

To understand lineage relationships between the cell clusters, we performed pseudotime analysis (**Figure 2E**). We found the cells to be part of a developmental lineage continuum that originates in the neural crest cell populations and transitions through a MIX pigment progenitor stage before differentiating into MI cells and MX cells, or Melanoblasts, consistent with a common origin for pigment cells(Bagnara et al., 1979; Petratou et al., 2021; Petratou et al., 2018). A branch point (demarcated as 3) emerged between melanoblasts and the MI and MX progenitors, indicative of two distinct melanoblast populations. This is consistent with our imaging analysis (**Figure 1**), which shows *mitfa*+ melanoblasts populations in the skin (before these become pigmented) and lining the nerves (which are relatively undifferentiated at that stage). Through RNA velocity analysis (La Manno et al., 2018), the developmental lineage relationships were found to be consistent with neural crest cells giving rise to MIX cell populations that can either differentiate towards a MX lineage, or initiate expression of melanocyte differentiation genes as either a MI progenitor (or even iridophore progenitors) or the more differentiated Melanoblast cell population (**Figure 2F; Figure S3**). Importantly, despite similar transcriptomes (**Figure 2D**), our analysis

indicate that the MI cells are not the progenitors differentiating into Melanoblast cells, suggesting that these represent two distinct of melanoblast formation in the zebrafish.

Identification of ErbB-dependent MSCs by scRNA-sequencing

Given that the MIX cell population were enriched for *mitfa*+ *crestin*+ double-positive cells (**Figure 2C-D**), it could function as a possible source for MSCs. Since MSCs are ErbB kinase dependent, we designed a scRNA-seq experiment in ErbB kinase inhibitor (ErbBi) treated *Tg(mitfa:GFP; crestin:mCherry)* transgenic embryos (**Figure 3A-B**). Clustering 347 cells derived from ErbBi-treated embryos revealed a loss of the MI cell population compared with our untreated dataset. Further, relative to melanoblasts from untreated embryos, the melanoblast population in ErbBi-treated embryos was enriched for cells with reduced differentiation markers, and we therefore called these cells Early Melanoblasts (**Figure 3B, Figure S4A**). Pseudotime analysis showed that cells from *Tg(mitfa:GFP;crestin:mCherry)* transgenic embryos form a developmental continuum from NCCs through MIX states to MX and Early melanoblast populations (**Figure 3C, Figure S4**). Interestingly, in contrast to a loss of cells in the MI lineage, *twist1a*$^{+}$ NCCs were proportionally increased in ErbBi-treated embryos whereas the early melanoblasts as well as the *twist1a*$^{+}$ NCCs were enriched for mesenchymal and proliferative markers including *zeb2a*, *ednrab*, *twist1a*, *pmp22a, pcna* (**Figure 3D, E; Figure S4B-C**) These data suggest that ErbB kinase signalling supports the transition from a migrating and proliferative NCC state toward a more established and stationary state.

We conclude from this data, combined with our imaging analysis, that the ErbB-dependent and nerve-associated progenitors represent MI cells lost upon ErbBi-treatment (**Figure 3C-E, Figure S4D**). However, from our UMAP, we could not easily distinguish a specific ErbB-dependent MIX subpopulation that represent MSCs (**Figure 3E**). To understand the hierarchical dependence of cells emerging from MIX progenitors, we performed an integrated pseudotime analysis between

untreated and ErbBi-treated embryos and reconstructed lineage trees. This approach enabled us to ask at which branch point ErbBi treatment would prevent ErbB-dependent generation of MSCs and MSC-derived cell populations, and how this would impact on MIX-derived cell populations (Qiu et al., 2017)(**Figure 3F**). In untreated embryos, cells distributed along the two main branches; the NCC lineage and the MSC lineage, which split into branches ending in defined states for axon-associated progenitors, the MIX population and directly developing melanoblasts. Between branches we could clearly see the pigment progenitors and the combined neural crest states, and the pigment progenitors and the combined pigment lineage. When comparing lineage trees of ErbBi-treated and untreated embryos, we observed that melanoblast-derived lineages were reduced overall and that axon-associated progenitors, robustly present in untreated embryos were almost entirely lost upon ErbBi treatment. In addition, cells obtained from ErbBi-treated embryos were largely deficient for transitioning cell states but enriched for *twist1a*$^{+}$ NCCs (**Figure 3F**), providing an explanation for the reduced number of *foxd3*+ NCC populations in the UMAP. Based on these data, we hypothesize that ErbB-dependent cells capable of transitioning between MIX and differentiating pigment cell lineages are MSCs. When we mapped these cells back to the untreated *Tg(mitfa:GFP; crestin:mCherry)* analysis, we found that the MSCs formed a subpopulation within the MIX cluster (**Figure 3G**), and that the MSCs in fact represent a branch point in the pseudotime analysis, supporting our hypothesis that their identity is a distinct cell state with the MIX cell population (**Figure 3H**).

tfap2b specifies MSC identity

Next, we performed a differential expression analysis comparing the transcriptomes between the putative MSCs and the combined pigment cell lineages derived from the same wild type embryos (**Figure 4A-B**). As anticipated for a MIX subgroup, MSCs expressed all the pigment progenitor markers (**Figure 4A, Table S3**), and combined pigment lineages were enriched for expression of

pigment synthesis genes, while the MSCs were enriched for expression of ribosome biogenesis and splicing genes, similar to what has been reported in other stem cell systems (Brombin et al., 2015; Gabut et al., 2020; Gupta and Santoro, 2020; Recher et al., 2013) (**Table S4**). Moreover, MSCs were enriched in genes involved in neurological disabilities in human patients when compared with the early pigment progenitors at the top of the lineage tree (**Table S5**).

Strikingly, we found *Transcription Factor AP-2 Beta* (*tfap2b)* to be the top gene specifically enriched within the transcriptome of the putative MSCs (**Figure 4A, B**). Tfap2b is a transcription factor, functionally redundant with Tfap2a, known to regulate neural crest and melanocyte development in mouse, and postulated to differentially specify melanocyte precursors together with Mitfa in zebrafish (Chong-Morrison and Sauka-Spengler, 2021; Lignell et al., 2017; Rothstein and Simoes-Costa, 2020; Seberg et al., 2017). In human melanoma cell xenograft studies, Tfap2b was identified as a marker of a subpopulation present in residual disease states following BRAF plus MEK inhibitor treatment (Rambow et al., 2018), and is also a marker of residual disease in our zebrafish melanoma models (Travnickova et al., 2019) (**Figure S5A**). To investigate whether Tfap2b plays a functional role in regulating the MSCs, we reproduced the Tfap2b (Biotin) ChIP-seq analysis carried out in chicken neural crest tissues (Ling and Sauka-Spengler, 2019). After mapping the chicken Tfap2b targets to their zebrafish homologs, we examined the expression of these genes in MSCs as well as the derivative cell populations within our dataset. We found that a select subset of Tfap2b targets are selectively highly expressed in MSCs compared to other cell states (**Figure 4C**, **Table S6**). These Tfap2b-MSC target genes are enriched in MIX cells derived from control embryos compared to MIX cells derived from ErbBi-treated embryos (**Figure 4D, Table S7**). These data suggest Tfap2b play a pivotal role in the specification of the MSC lineage through activation of a select set of Tfap2b target genes.

tfap2b is expressed at the MSC niche and required for regeneration

Next, we asked if *tfap2b* is functionally important for MSC-derived melanocytes but not for melanocytes emerging directly from the neural crest. To answer this question, we used a melanocyte regeneration assay based on a temperature-sensitive *mitfa* mutation, (*mitfa*^{vc7}), in which embryos are incapable of generating embryonic melanocytes at higher temperatures, but capable of regenerating melanocytes from MSCs at lower temperatures (Johnson et al., 2011; Zeng et al., 2015). We found that morpholino (MO)-mediated knockdown of *tfap2b* did not impact on the development of most NC-derived melanocytes, but significantly reduced MSC-derived melanocytes in regeneration (**Figure 5A**). These results were confirmed with a second, splicing-site MO knockdown (**Figure 5A**). Because MSCs contribute to a small population of melanocytes in the embryonic lateral stripe pattern, MSC activity in zebrafish embryos can be assessed through this second independent assay. Indeed, in *tfap2b* knockdown embryos, we found MSC-derived late-stage lateral stripe melanocytes to be reduced, confirming that *tfap2b* is required for MSC-derived melanocyte populations even in non-regenerating embryos (**Figure 5B**).

Having established a function for *tfap2b* in MSC-derived lineages, we next sought to visualise *tfap2b* MSCs during development. To this end, we isolated a 1kb *tfap2b* promoter region and cloned it upstream of the *eGFP* coding sequence to generate a transgenic reporter line *Tg(tfap2b:eGFP),* and then crossed this line with *Tg(crestin:mCherry)* animals. In double transgenic animals, we identified cells co-expressing GFP and mCherry at the MSC niche and along nerves. Critically, these cells were absent during ErbBi treatment, indicating that *Tg(tfap2b:eGFP)* expression marks the MSC lineage (**Figure 5C-E**).

In extended imaging analysis, we revealed that *Tg*(*tfap2b:eGFP)* expression peaked during the first 48 hpf but then declined with *crestin:mCherry* expression. We saw no overt evidence of *tfap2b:eGFP* expression in adult zebrafish pigment cells, although expression was sustained in the spinal cord in accordance with a neuronal expression pattern (Knight et al., 2005). We did not

find evidence of *tfap2b:eGFP* expression in other embryonic melanocytes or pigment cells by imaging, and analysis of our and other datasets confirmed that *tfap2b* expression is restricted to the MSC population in the pigment cell lineage (**Figure S5B-C**). Together, these results indicate that Tfap2b transiently functions to establish MSC identity during embryogenesis. Thus, Tfap2b plays a role in MSC identity acquisition that is critically required during the first few days of embryonic development.

tfap2b+ MSCs have multi-fate potential for all adult pigment cell lineages

MIX cells can give rise to the entire complement of pigment cells within a hemisegment (Singh et al., 2016). The highly specific *tfap2b* gene expression in MSCs (**Figure S5B-C**) prompted us to follow the fate of *tfap2b*+ cells. To this end, we cloned the 1kb promoter upstream of *CRE* (*tfap2b:CRE*) and injected it into the *ubi:switch* transgenic line, which can be used for the lineage tracing of cells recombined from GFP+ to RFP+ ("switched") cells (Mosimann et al., 2011) (**Figure 6A-F**). Injected zebrafish embryos were mosaic for *tfap2b:CRE* integration thereby facilitating the tracing of clones that originated from a single or few recombination events.

Tfap2b is expressed in neural cells in development (Knight et al., 2005), and consistent with this, we found RFP^+ neurons in the dorsal neural tube as soon as 48hpf (**Figure 6B**, **Figure S5C**). Critically, by 6 days of development, we found RFP^+ MSCs at the niche and in a few melanocytes in the skin. By 13 dpf, we could clearly detect RFP^+ MSCs and nerve associated cells, melanocytes and xanthophores. By 1 mpf, RFP^+ melanocytes, xanthophore and iridophores were particularly prominent in the developing stripes during metamorphosis (**Figure 6E-H**). At this stage, MIX clones spanned the whole dorso-ventral axis in hemisegments and were clearly visible in the scales. We did not observe clones composed of a single pigment cell type (*e.g.* only melanocytes, iridophores or xanthophores), indicating that *tfap2b*+ cell were not yet fate restricted. While most fish had MIX clones that filled the hemisegment stripes (**Figure 6G, H**) we

observed one fish with a sparse clone made up of only a few iridophores, xanothophores and melanocytes distributed along the length of the hemisegment and not adjacent to each other (**Figure 6F**). This may indicate that MSCs do not all have equal potential to generate progenitors or may represent a late-stage MSC activation event. Some very large clones spanned one or more segments along the rostro-caudal axis indicating that the CRE recombination might have occurred in one or more consecutive MSCs.

These findings confirm that *tfap2b* labels established MSC populations at the niche, and that these cells have a MIX identity that gives rise to all three late-stage developmental and adult pigment cell types.

Discussion

MSCs provide an on-demand source of melanocytes during growth, metamorphosis and regeneration, however, we have lacked an understanding of how MSCs are specified from the neural crest or melanocyte progenitors in embryogenesis. Here, we discovered that Tfap2b is a functional marker for MSCs during specification and regeneration, and that MSCs are fated to contribute to all three pigment cell lineages in the adult zebrafish. Conceptually, our scRNA-sequencing analysis supports a model in which MIX cells give rise to either MI progenitors, that have melanocyte and iridophore potential, or MX progenitors, that have melanocyte and xanthophore potential (Nusslein-Volhard and Singh, 2017; Singh et al., 2016). Our lineage tracing analysis proves that *tfap2b*+ MSCs are multi-potent and give rise to melanocytes, iridophores and xanthophores of the adult. Further, our findings molecularly resolve two developmental pathways for melanocytes; melanoblasts, that develop directly from the neural crest, and MI cells, that line the nerves and remain relatively undifferentiated. These findings provide a foundation for studying how MSCs are specified from the neural crest and shape animal pigmentation patterns.

The existence of MSCs in zebrafish was proposed in melanocyte regeneration assays, in which melanocyte populations were replenished by an ErbB kinase-dependent population following ablation of pigmented melanocytes (Hultman et al., 2009; Hultman and Johnson, 2010; Johnson et al., 2011; O'Reilly-Pol and Johnson, 2009). ErbB kinase inhibitors or genetic mutation only affected a discrete population of embryonic lateral stripe melanocytes, however in the adult fish, large segments of the adult stripe pattern were absent (Budi et al., 2008; Dooley et al., 2013; Hultman et al., 2009; Hultman and Johnson, 2010). Immunohistochemistry and live-imaging analysis showed that MSCs localized at the DRG and that undifferentiated *mitfa*+ cells lined the peripheral nerves (Budi et al., 2011; Dooley et al., 2013; Johansson et al., 2020). Additional MSC populations may be present in the zebrafish embryo, including an ErbB-dependent and blood vessel-associated population dependent on Endothelin factors (Camargo-Sosa et al., 2019). Despite expressing *mitfa*, MSCs do not exclusively require Mitfa activity for their establishment (Johnson et al., 2011). Mitfa has been proposed, however, to function with other Tfap2 family members such as Tfap2b to promote the expression of melanocyte genes (Seberg et al., 2017). Our data supports a new model in which Tfap2b regulates expression of a select set of target genes required for MSC specification, and after which melanocyte differentiation is governed by Mitfa.

Despite the strong functional evidence for MSC activity at the DRG, the lack of cell type-specific markers have prevented investigations into molecular mechanisms underpinning their biology. Further, although MSCs are anatomically similar to the SCP cell population in mammals (Adameyko et al., 2009; Budi et al., 2011; Dooley et al., 2013), there have been few tools to study this population in development, regeneration or adult tissues. Our findings that *tfap2b* expression specifically marks the MSCs should facilitate the direct isolation and further characterisation of how MSCs relate to SCP cells, and how nerves provide a niche for melanocyte progenitors (Furlan and Adameyko, 2018).

As one of the most aggressive and heterogenous cancers, the melanoma transcriptional landscape spans developmental neural crest and melanocyte lineage signatures, stem cell signatures, and trans-differentiation signatures (Diener and Sommer, 2020; Marine et al., 2020; Patton et al., 2021). We propose that the molecular mechanisms that regulate MSC biology have direct relevance to melanoma pathogenesis. Illustrating this, we recently discovered that the rate of differentiation from the MSC lineage in zebrafish is dependent on a PRL3-DDX21 transcriptional elongation checkpoint and that this same mechanism in melanocyte regeneration portends poor outcomes for melanoma patients (Johansson et al., 2020). Importantly, we and others find that Tfap2b is expressed in human and zebrafish melanoma residual disease cell states, a malignant and drug-resistant cell state that contributes to disease recurrence (Marine et al., 2020; Rambow et al., 2018; Shen et al., 2020; Travnickova et al., 2019) (**Figure S5A**). Thus, the developmental Tfap2b mechanism we identify here for zebrafish MSCs could be co-opted in melanoma, such that Tfap2b melanoma residual disease cell states may represent a dysregulated MSC developmental lineage.

Author Contributions

Conceptualization: EEP, AB; Methodology: AB, JT; Software: AB, DJS, JT, YL; Validation: AB, HB, ZQ; Formal analysis: AB, DJS, YL; Investigation: AB, JT, HB, ZZ; Resources: EEP; Writing original draft : EEP, AB; Writing review and editing: All authors; Visualisation: AB; Supervision: EEP, TC; Funding acquisition: EEP, TC

Declaration of Interests

The authors declare no competing interests.

Acknowledgements

We are grateful to Cameron Wyatt and the IGC Zebrafish Facility for zebrafish management and husbandry, Elisabeth Freyer and the IGC FACS facility, Ann Wheeler and the IGC Imaging Facility for supporting the imaging experiments, Edinburgh Genomics for sequencing, Christina Lilliehook for editing support, and Lauren Saunders and David Parichy for helpful discussions on scRNA-sequencing analysis. DJS is funded by the Medical Research Council (Doctoral Training Programme in Precision Medicine). TC is funded through a Chancellor's fellowship held at the University of Edinburgh. EEP is funded by MRC HGU Programme (MC_UU_00007/9), the European Research Council (ZF-MEL-CHEMBIO-648489), and Melanoma Research Alliance (687306).

FIGURE LEGENDS

Figure 1: MSCs maintain a neural crest identity at the niche.

A. Schematic of developing MSC melanocyte lineages in the zebrafish embryo. *mitfa* expressing melanoblasts (Mbs; green) develop directly from the neural crest and travel to the skin either dorsolateraly (not shown) or ventrally along the neural tube (NT) and peripheral nerves (red; **B**). A subset of those cells, establish at the site of the of the perspective DRG and become MSCs (blue cell, **C**). MSCs establishment is sensitive to ErbB-kinase inhibitors (ErbBi).

B. Melanoblasts migrating along the axons at the neural tube.

C. Newly established MSC at the site of a perspective DRG. Confocal stack (20 μm) of *Tg(mitfa:GFP; nbt:dsRed)* embryo imaged laterally at 22 hpf. Scale bar: 20 μm.

D. ErbB kinase activity is required for MSCs establishment at the stem cell niche (white arrow). Confocal stacks (20 μm) of *Tg(mitfa:GFP; nbt:dsRed)* embryos treated with either 0.05% DMSO or 5 μM ErbBi. Standard deviation projection. Scale bar: 20 μm.

E. Quantification of MSC niche occupancy. Tukey-HSD (Honestly Significant Difference) test. ***: p-value <0.0001.

F. MSCs maintain neural crest identity at the niche. Confocal stacks (30 μm) of *Tg(crestin:mCherry; mitfa:GFP)* embryos treated with either 0.05% DMSO or 5 μM ErbBi. MSCs (white arrows) and nerve-associated cells (yellow arrows) are dependent on ErbB-kinase. Standard deviation projection. Scale bar: 20 μm.

G. MSCs and nerve associated precursors express *mitfa:GFP* and *crestin:mCherry*, but expression is lost by 120 hpf. Confocal stacks (30 μm) of *Tg(crestin:mCherry; mitfa:GFP)* embryos. The lower edge of the neural tube is indicated (white dotted line) on both fluorescent

and corresponding brightfield images (top panels). Brightfield images: average intensity projections; fluorescent images: standard deviation projection. Scale bar: 50 μm.

Figure 2. scRNA-seq identifies six distinct neural crest-pigment cell lineage populations.

A. Schematic of the experimental protocol. Cells that express GFP, mCherry or both were isolated from *Tg(crestin:mCherry; mitfa:GFP)* embryos at 24 hpf.

B. UMAP of GFP+, mCherry+ and double GFP+ mCherry+ cells (n = 996 cells) obtained from 24 hpf zebrafish embryos after Louvain clustering (dims= 20, resolution = 0.5).

C. Heatmap showing the average log_2-fold change expression of five selected genes per cluster identified in **B**. The average log_2-fold change expression across the 6 clusters of *sox10*, *crestin*, *mitfa*, *mCherry* and *eGFP* expression levels are also presented for comparison.

D. UMAP representations of **B** with color change from grey (negative) to red (positive) based on log_2 mRNA expression of *pcna*, *twist1a*, *foxd3*, *aox5*, *mitfa*, and *tyrp1b*.

E. Pseudotime ordering of cells in **B**. Top panel: cells are colored according to their pseudotime scores; bottom panel: cells are colored according to their cluster identity.

F. RNA velocity analysis of the UMAP represented in **B** (top panel) and simplified representation of the same results (bottom panel).

Figure 3. Identification of ErbB-dependent MSCs by scRNA-sequencing

A. Schematic of scRNA-seq experimental protocol for ErbBi-treated zebrafish embryos (24 hpf). 5μM ErbBi treatment: 4 - 24hpf.

B. UMAP of GFP+, mCherry+ and GFP+ mCherry+ double positive cells (n = 346 cells) obtained from ErbBi-treated zebrafish embryos after Louvain clustering (dims = 10, resolution = 0.5).

C. Pseudotime ordering of cells in **B**. Left panel: cells are colored according to their pseudotime scores; right panel: cells are colored according to their cluster identity.

D. UMAP of GFP+, mCherry+ and double GFP+ mCherry+ cells (n=1343 cells) from untreated and ErbBi-treated embryos after Louvain clustering (dims = 12, resolution = 1).

E. UMAP representations of **D** pseudocolored with the origin of the cells analysed. Dashed lines highlight clusters enriched with ErbBi-treated cells.

F. Lineage tree representation of the pseudotime ordering of combined datasets. Progenitor states present in the untreated embryos (dashed box) are absent in ErbB inhibitor treated embryos (arrow). Cells are pseudo-colored according to their cluster of origin. Cell states and the inferred cellular position in the 24 hpf embryo are indicated.

G. ErbB-kinase dependent MSCs (red) and the MI progenitors (brown) are highlighted on UMAP presented in **2B**.

H. Minimum spanning tree presented in **2E** (cells from untreated embryos) pseudocolored according to the cell states described in the lineage trees (**F**)**.** The inferred cellular position and the MSC branch point are indicated.

Figure 4. *tfap2b* specifies MSC identity

A. Violin plots of pigment progenitor and MSC gene expression levels. MSCs differentially express a subset of genes (MSC genes) and share expression of genes with cells of the pigment cell lineage (Early pigment progenitors, MI, MX and Melanoblasts from untreated embryos in **Figure 3F**; **Table S3**).

B. Rank plot of differential expression analysis between MSCs and all other states of the pigment lineage. The top differentially expressed gene is *tfap2b* (log_2 fold change: 5.63; adjusted p-value: $4.99e^{-5}$; **Table S3**).

C. Clustered heatmap showing the average expression of 36 Tfap2b targets enriched in the MSCs and 3 non-differentially expressed targets (**Table S6**).

D. Rank plot of differential expression analysis between MIX cells between untreated embryos and ErbBi-treated embryos. Most of the MSC-Tfap2b target genes are depleted from MIX cells in ErbBi-treated embryos (**Tables S6, S7**).

Figure 5. *tfap2b* is expressed at the MSC niche and required for regeneration

A. *tfap2b* is required for melanocyte regeneration from the MSC. Images of zebrafish embryos and melanocyte quantification following knock-down of *tfap2b* in a *mitfa*^{vc7} regeneration assay. Tukey-HSD (Honestly Significant Difference) test; ***: p-value <0.0001. Scale bar: 200μm. N.I.: Not injected; Co. MO: Control morpholino; AUG MO: AUG-directed morpholino; Splic. MO: Splicing morpholino. Representative of 3 repeated experiments.

B. *tfap2b* is required for late-stage melanocytes from the MSC. Images of zebrafish embryos and melanocyte quantification following knock-down of *tfap2b*. Only MSC-derived late-developing lateral stripe melanocytes are reduced in *tfap2b* knockdown embryos. Arrows highlight missing lateral stripe melanocytes. Tukey-HSD (Honestly Significant Difference) test; ***: p-value <0.0001. Scale bar: 200μm. Representative of 3 repeated experiments.

C. Transgenic *tfap2b:eGFP* expression in the MSC. Merged Image of a double transgenic *Tg(tfap2b:eGFP; crestin:mCherry)* zebrafish (left panel) and separated channel images (brightfield, GFP and mCherry channel). White arrows indicate GFP+/mCherry+ double positive MSCs at the DRG. Scale bar: 50μm.

D. *tfap2b*+ MSCs require ErbB-kinase at the niche. *Tg(tfap2b:eGFP;crestin:mCherry)* embryos at 24 hpf (**D**) and 48 hpf (**E**), either untreated or with 5 μM ErbBi. White arrows indicate MSC niche. Tukey-HSD (Honestly Significant Difference) test; *: p-value=0.0172, ***: p-value <0.0001. Representative of 3 repeated experiments. Confocal stacks (30 μm). Standard deviation projection. Scale bar: 50 μm.

Figure 6. *tfap2b*+ MSCs have multi-fate potential for all adult pigment cell lineages

A. Experimental protocol overview for *tfap2b*+ mosaic lineage tracing. *pEXP-GC2Tol2-tfap2b:CRE* and *Tol2* mRNA were injected in *ubi:switch* embryos at the zygote stage and imaged at different stages to identify RFP expressing melanocytes.

B - D. *tfap2b* lineage tracing analysis during zebrafish development. **B:** 48 hpf, **C:** 6 dpf, **D**: 13 dpf. Representative images of 7-8 embryos/larvae imaged per stage. White pseudo-coloring is used for the RFP channel. M: melanocytes; MSCs: melanocyte stem cell; N: spinal cord neurons; X: Xanthophore. Maximum Intensity projection. Scale bars: 50μm.

E - H. MIX clones in *tfap2b* lineage tracing analysis in adult zebrafish. **E:** SL 14.2 mm, caudal trunk; **F,** SL 11.4 mm, tail; **G**, SL 12.3 mm, medial trunk; **H**, SL 11.3 mm, caudal trunk. Magnified images of melanocytes in stripe 2D (**E'**, **E''**), in stripe 1D (**E''**). **F** depicts a sparse MIX clone, with magnifications of iridophores, xanthophores and a melanocyte (from top to bottom). **G-H** show MIX clones spanning the dorso-ventral axis. White pseudo-coloring is used for the GFP channel and red is used for the RFP channel in **E-H**; white pseudo-coloring is used for the RFP channel in magnified panels in **E** and **F**. Representative images of 2 imaging sessions (each derived from a single injection section) of 1mpf-old fish (7 fish per imaging session). I.s.: Interstripe, St.:Stripe. Maximum Intensity projection. Scale bars: 50 μm.

KEY RESOURCES TABLE

REAGENT or RESOURCE	SOURCE	IDENTIFIER
Chemicals, Peptides, and Recombinant Proteins		
AG1478	Calbiochem/Sigma-Aldrich	Cat No: #658552
FACSMax	AMSbio	Cat No: AMS.T200100
(+/-) – Epinephrine hydrochloride	Sigma-Aldrich	Cat No: E4642-5G
Commercial Assays		
Chromium Single Cell 3' Library & Gel Bead Kit v2, 16rxns	10x Genomics	Cat No: PN-120237
Chromium Single Cell A Chip Kit, 16 rxns	10x Genomics	Cat No: PN-10000009
Chromium i7 Multiplex Kit, 96 rxns	10x Genomics	Cat No: PN-120292
Tol2kit gateway cloning	(Kwan et al., 2007) http://tol2kit.genetics.utah.edu/index.php/Main_Page	N/A
Deposited Data		
scRNA-seq data	This paper	GEO# pending
Zebrafish single cell RNA-seq – 1 dpf	(Wagner et al., 2018) https://www.ncbi.nlm.nih.gov/geo/query/acc.cgi?acc=GSM3067195)	GEO # GSE112294 /GSM3067195
Zebrafish single cell RNA-seq – 1 dpf	(Saunders et al., 2019) https://www.ncbi.nlm.nih.gov/geo/query/acc.cgi?acc=GSE131136	GEO # GSE131136 /GSM3764579
Zebrafish single cell RNA-seq – 5 dpf	(Farnsworth et al., 2020) http://cells.ucsc.edu/?ds=zebrafish-dev	NCBI SRA # PRJNA564810
Zebrafish melanoma datasets	(Travnickova et al., 2019)	GEO # GSE136900
Tfap2b (biotin) ChIP-seq	(Ling and Sauka-Spengler, 2019)	GSE125711
Experimental Models: Organisms/Strains		
mitfa$^{vc7/vc7}$	(Johnson et al., 2011)	RRID:ZFIN_ZDB-GENO-110330-3

Tg(nbt:dsred) – Tg(Xla.Tubb:dsred)	Professor David Lyons Edinburgh University	ZFIN Cat #: ZDB-TGCONSTRCT-081023-2
Tg(mitfa:gfp)	(Dooley et al., 2013)	ZFIN Cat #: ZDB-TGCONSTRCT-081203-1
Tg(crestin:mCherry)	This paper from plasmid generated by Kaufman and colleagues (Kaufman et al., 2016)	ZFIN Cat #: ZDB-TGCONSTRCT-160208-3
Tg(ubi:loxP-EGFP-loxP-mCherry) - ubi:Switch	(Mosimann et al., 2011)	ZFIN Cat #: ZDB-FISH-201123-10
Tg(tfap2b:eGFP)	This paper	N/A
Tg(tfap2b:CRE)	This paper	N/A
Oligonucleotides:		
tfap2b promoter F 5'-GGGGACAACTTTGTATAGAAAAGTTGtacccagagagtcacacatgg-3'	Sigma-Aldrich	N/A (custom made)
tfap2b promoter R 5'-GGGGACTGCTTTTTTGTACAAACTTGtGGAATACGCGTGCACTAACAT-3'	Sigma-Aldrich	N/A (custom made)
CRE cds F 5'-ggggacaagtttgtacaaaaaagcaggcttcGCCACCATGCCCAAGAAGAAGAGGAAG-3'	Sigma-Aldrich	N/A (custom made)
CRE cds R 5'-ggggaccactttgtacaagaaagctgggtcttCTAATCGCCATCTTCCAGCAG-3'	Sigma-Aldrich	N/A (custom made)
tfap2b MO (AUG-directed): 5'- CGTGCACTAACATCTGGGCGGAAAA-3'	GeneTools LLC	N/A (custom made)
tfap2b MO (Splicing site-directed): 5'- GGTGGAAATAATGATAGTCTCACCT-3'	GeneTools LLC	N/A (custom made)
Standard control morpholino	GeneTools LLC	N/A
Recombinant DNA		
pDONOR221	Tol2kit v1.2	plasmid #:218
pDONRP4-P1R	Tol2kit v1.2	plasmid #:219
p5E-actin2	Tol2kit v1.2	plasmid #:299
p3E-polyA	Tol2kit v1.2	plasmid #:302
pME-eGFP	Tol2kit v1.2	plasmid #: 383
pDestTol2pA2	Tol2kit v1.2	plasmid #: 394
pDestTol2CG2	Tol2kit v1.2	plasmid #:395
p5E:tfap2b	This paper	N/A
p5E:CRE	This paper	N/A
pEXP(tfap2b:GFP)	This paper	N/A
pEXPGC2(tfap2b:CRE)	This paper	N/A
Software and Algorithms		

CellRanger (v.2.1.1)	10x Genomics	RRID:SCR_017344
Scater (v.1.12.2)	(McCarthy et al., 2017) https://bioconductor.org/packages/release/bioc/html/scater.html	RRID:SCR_015954
Scran (v.1.12.1)	(Lun et al., 2016) https://bioconductor.org/packages/release/bioc/html/scran.html	N/A
Seurat (v.2.3.4)	(Butler et al., 2018) https://satijalab.org/seurat/	RRID:SCR_016341
Seurat (v.3.1.4)	(Stuart et al., 2019) https://satijalab.org/seurat/	RRID:SCR_016341
scDE (v.1.99.4)	(Kharchenko et al., 2014) https://hms-dbmi.github.io/scde/	RRID:SCR_015952
Monocle (v.2.12.0)	(Trapnell et al., 2014) http://cole-trapnell-lab.github.io/monocle-release/docs/	RRID:SCR_016339
ClusterProfiler (v.3.12.0)	(Yu et al., 2012) https://bioconductor.org/packages/release/bioc/html/clusterProfiler.html	RRID:SCR_016884
Velocyto R package (v.0.6)	(La Manno et al., 2018) http://velocyto.org/	RRID:SCR_018167
ChIPseeker (v.1.26.2)	(Yu et al., 2015) https://bioconductor.org/packages/release/bioc/html/ChIPseeker.html	N/A
Homologene (v1.5.68.21.2.14)	http://www.ncbi.nlm.nih.gov/homologene	RRID:SCR_002924
ggPlot2 (v.3.2.1)	(Wickham, 2016) https://cran.r-project.org/web/packages/ggplot2/index.html	RRID:SCR_014601

R (v.3.6.2)	http://www.r-project.org/	RRID:SCR_001905
RStudio (v.2)	http://www.rstudio.com/	RRID:SCR_000432
Micromanager (Version 1.4)	http://micro-manager.org	RRID:SCR_00041
Fiji 1.0	http://fiji.sc	RRID:SCR_002285

STAR METHODS

RESOURCE AVAILABILITY

Lead contact

Further information and requests for resources and reagents should be directed to and will be fulfilled by the Lead Contact, E. Elizabeth Patton (e.patton@ed.ac.uk).

Materials availability

Newly generated materials from this study are available upon request to the Lead Contact, E. Elizabeth Patton (e.patton@ed.ac.uk).

Data and code availability

scRNA-seq experiments have been submitted to GEO: GEO # pending at the moment of submission. All other data and codes supporting the findings of this study are available from the Lead contact (e.patton@ed.ac.uk) upon reasonable request.

EXPERIMENTAL MODELS

Zebrafish were maintained in accordance with UK Home Office regulations, UK Animals (Scientific Procedures) Act 1986, amended in 2013, and European Directive 2010/63/EU under project license 70/8000 and P8F7F7E52. All experiments were approved by the Home office and AWERB (University of Edinburgh Ethics Committee).

Fish stocks used were: wild-type AB, *mitfa*^{vc7} (Johnson et al., 2011; Zeng et al., 2015) , *Tg(nbt:dsRed), Tg(mitfa:GFP)* (Dooley et al., 2013), *Tg(crestin:mCherry)*(Kaufman et al., 2016) (generated for this study from the plasmid kindly provided from Richard Kaufman, University of Washington), *Tg(ubi:loxP-EGFP-loxP-mCherry) (ubi:Switch*) (Mosimann et al., 2011), *Tg(tfap2b:GFP)* (this study). Combined transgenic and mutant lines were generated by crossing. Adult fish were maintained at ~28.5°C under 14:10 light:dark cycles. Embryos were kept at either 25°C, 28.5°C or 32°C and staged according to the reference table provided by Kimmel and colleagues (Kimmel et al., 1995) or Parichy and colleagues (Parichy et al., 2009)

METHODS

Generation of zebrafish transgenic lines

The promoter region of *tfap2b* (1kb upstream of the first coding exon) was PCR amplified from zebrafish total genomic DNA with the following set of primers: forward: 5'-GGGGACAACTTTGTATAGAAAAGTTGtacccagagagtcacacatgg-3'; reverse: 5'-GGGGACTGCTTTTTTGTACAAACTTGtGGAATACGCGTGCACTAACAT-3'. Amplicons were cloned into *pDONRP4-P1R* (Tol2Kit v1.2, plasmid #: 219) to generate the *p5E-tfap2b* entry clone which were combined with either *pME-eGFP* (Tol2Kit v1.2, plasmid #: 383) (Kwan et al., 2007), and the SV40 polyA sequence from *p3E-polyA* (Tol2Kit v1.2, plasmid #: 302) into the

pDestTol2pA2 (Tol2Kit v1.2, plasmid #: 394) destination vector to generate *pEXP(tfap2b:GFP)* and expression vectors.

The CRE coding sequence was amplified from *pMC-CreN* plasmid (kind gift Jianguo Shi Check) with the following primers: forward: 5'-ggggacaagtttgtacaaaaaagcaggcttcGCCACCATGCCCAAGAAGAAGAGGAAG-3'; reverse 5'-ggggaccactttgtacaagaaagctgggtcttCTAATCGCCATCTTCCAGCAG-3'. The amplicon was cloned into *pDONOR221*(Thermo Fisher) producing a middle entry vector, *pME-CRE* that was cloned with the *tfap2b* promoter from *pME-tfap2b* , and the SV40 polyA sequence from p3E-polyA into the *pDestTol2CG2* destination vector (Tol2Kit v1.2, plasmid #: 395) to generate the *pEXPGC2(tfap2b:CRE)* expression vector.

The pEXP vectors were mixed with *Tol2* mRNA (in vitro transcribed with the Ambion mMessage mMachine SP6 Kit, Thermo Fisher, from the Tol2Kit *pCS2FA-transposase* plasmid – plasmid #: 396); and microinjected into 1-cell stage either AB or *ubi:switch* embryos, at a final concentration 25 ng/µl and 35 ng/µl respectively. Zebrafish embryos expressing the transgenes were selected and grown to adulthood before crossing with wildtype zebrafish to obtain the F1 generation.

Zebrafish morpholino oligonucleotides

For the *tfap2b* morpholino, 1ng of AUG-directed morpholino (5'-CGTGCACTAACATCTGGGCGGAAAA-3') or 2ng of splicing morpholino (5'-GGTGGAAATAATGATAGTCTCACCT-3') oligonucleotide were injected, as well as the standard control (Gene Tools, LLC). Regenerating melanocytes in *tfap2b* morpholino-injected and control-injected fish were tested in the *mitfa*^{vc7} regeneration assays with embryos raised at 32°C for 72h before down-shifting to 25°C. Quantification and imaging of regenerating melanocytes at 120 hpf. Late-developing melanocytes in *tfap2b* morpholino-injected and control-injected fish were tested

during normal development in AB embryos raised at 28.5°C for 120h before quantification and imaging of regenerating melanocytes at 120 hpf. Representative of 3 biological replicates.

Imaging

Embryos at 4 hpf *Tg(mitfa:GFP; nbt:dsRED)*, *Tg(mitfa:GFP; crestin:mCherry) or Tg(tfap2b:GFP; crestin:mCherry)* were arrayed in 6-well plates (Corning) containing 0.05% DMSO or 5 μM AG1478 (ErbB-inhibitor, ErbBi, Sigma-Aldrich) in 3 ml of E3 embryo medium and kept at 28°C until imaging time. *ubi:swit*ch embryos injected with *pEXPGC2(tfap2b:CRE)* were screened under a fluorescence stereomicroscope for the presence of GFP in the heart at 48 hpf and were then raised as described previously. Embryos or fish were selected randomly for confocal imaging as above. Fish older than 5 dpf were imaged while in terminal anaesthesia. 1mpf fish were first imaged were soaked in 5mg/ml epinephrine (Sigma-Adrich) for 10 minutes prior mounting in low-melting point agarose. Images of randomly picked embryos or selected adult fish were acquired using a 0.4x/0.3, a 10X/0.5 or a 20X/0.75 lens on the multimodal Imaging Platform Dragonfly (Andor technologies, Belfast UK) equipped with 405, 445, 488, 514, 561, 640 and 680nm lasers built on a Nikon Eclipse Ti-E inverted microscope body with Perfect focus system (Nikon Instruments, Japan). Data were collected in Spinning Disk 40μm pinhole mode on the Zyla 4.2 sCMOS camera using a Bin of 1 and no frame averaging using Andor Fusion acquisition software. If required: Z stacks were collected using the Nikon TiE focus drive. Multiple positions were collected using a Sigma-Koki Stage (Nikon Instruments Japan).

For melanocyte counting, regenerating and normal developing embryos were fixed in 4% PFA/PBS and dehydrated in increasing concentrations of glycerol (Sigma-Adrich). Images were acquired Leica MZFLIII fluorescence stereo microscope with a 1x objective fitted with a Qimaging Retiga Exi CCD camera (Qimaging, Surrey, BC, Canada). Image capture was performed using Micromanager (Version 1.4).

Data were analysed using Fiji 1.0 and 64bit Java8. Representative of 3 biological repeats.

Single cell suspensions, fluorescence activated cell sorting and library preparation

Tg(mitfa:GFP; crestin:mCherry) were processed in two instances and the following method had been applied to each treatment separately to obtain 2 libraries.

300 – 400 embryos at 4 hpf were divided in two equally sized batches and arrayed in 6-well plates (Corning) containing either E3 or 5 μM AG1478 (ErbBi) in 3 ml of E3 till 24hpf. A single cell suspension of each batch of embryos was then produced following the method described by Manoli and colleagues (Manoli and Driever, 2012) with minor modifications. Samples were sorted by a FACSAria2 SORP instrument (BD Biosciences UK). Green fluorescence was detected using GFP filters 525/50 BP and 488 nm laser, red fluorescence was detected using RFP filters 582/15 BP and 561 nm laser, and live cells selected with DAPI using DAPI filters 450/20 BP and 405 nm laser. Prior to sorting for fluorescence levels, single cells were isolated by sequentially gating cells according to their SSC-A vs. FSC-A and FSC-H vs FSC-W profiles according to standard flow cytometry practices. Cells with high levels of DAPI staining were excluded as dead or damaged. Cells from wild-type stage matched embryos (without transgenes) were used as negative control to determine gates for detection of mCherry and GFP fluorescence. Then *Tg(mitfa:GFP; crestin:mCherry)* cells from either untreated or ErbBi-treated zebrafish were purified according to these gates. 10,000 (AB background) fluorescent cells per batch were collected in 100μl of 0.04% Bovine Serum Albumin (BSA)/PBS in LoBind tubes (Fisher Scientific), spun down at 300G at 4°C, resuspended in 34μl of 0.04% BSA/PBS, and immediately processed using the Chromium platform (10x Genomics) with one lane per sample. Single-cell mRNA libraries were prepared using the single-cell 3' solution V2 kit (10x Genomics). Quality control and quantification assays were performed using High Sensitivity DNA kits on a Bioanalyzer (Agilent).

Libraries were sequenced on an Illumina NovaSeq platform (1 lane of a S2 flowcell, read 1: 26 cycles, i7 Index: 8 cycles, read 2: 91 cycles). Each sample was sequenced to an average depth of at least 1750 million total reads. This resulted in an average read depth of ~50,000 reads/cell after read-depth normalisation.

QUANTIFICATION AND STATISTICAL ANALYSIS

Statistical details of the experiments, n numbers, and dispersion and precision measurements can be found in the figure legends.

Bioinformatics analysis

scRNA-seq data processing and quality check

FastQ files were aligned using the CellRanger (v.2.1.1, 10x Genomics) pipeline to custom zebrafish STAR genome index using gene annotations from Ensembl GRCz11 release 94 with manually annotated entries for *eGFP*, *mCherry*, *mitfa* intron 5 and *mitfa* intron 6 transcripts, filtered for protein-coding genes (with Cell Ranger *mkgtf* and *mkref* options). Final cellular barcodes and UMIs were determined using Cell Ranger. Libraries were aggregated (using 10X Cell Ranger pipeline 'cellranger aggr' option), with intermediary depth normalization to generate a gene-barcode matrix.

Gene-cell matrices (total: 1519, from untreated embryos: 1022, from ErbBi-treated embryos: 497) were uploaded on R (v.3.6.2) and standard quality control metrics with the Scater package (v.1.12.2)(McCarthy et al., 2017). Only cells with total features >700, log10 total counts > 3.0, and mitochondrial gene counts (%) < 10 were considered as high quality and kept for further analyses (total:1343, from untreated embryos: 996, from ErbBi-treated embryos: 347). Prediction of the cell cycle phase was performed using the cyclone function in the Scran (v.1.12.1) (Lun et al., 2016).

Clustering, UMAP visualisation and cluster calling

The Louvain clustering of the separated libraries (**Figure 2B, 3B**) was performed with Seurat (v.3.1.4) (Stuart et al., 2019) using the *FindNeighbors* and *FindClusters* functions (cells from untreated embryos: dims = 20, resolution = 0.5; cells from ErbBi-treated embryos: dims = 10, resolution = 0.5) after performing linear dimensionality reduction and checking the dimensionalities of the datasets visualised with elbow plots.

Data were projected onto 2 dimensional spaces using Uniform Manifold Approximation and Projection (UMAP) (McInnes et al., 2018) using the same dimensionality values listed above.

Cluster specific genes were identified using the *FindAllMarkers* and *FindMarkers* function in Seurat (v.2.3.4 or v.3.1.4) with default parameters (Wilcoxon Rank Sum test that compares a single cluster against the others) and then using a Bayesian approach with the scDE package (v.1.99.4) (Kharchenko et al., 2014). See **Table S2**.

Cluster calling was done after detection of published marker genes for specific cell types and by making unbiased pairwise comparisons based on gene overdispersion against published datasets GEO #: GSE112294 (Wagner et al., 2018), GEO #: GSE131136 (Saunders et al., 2019), and NCBI SRA #: PRNJNA56410 (Farnsworth et al., 2020) using the scMap package (v.1.6.0) (Kiselev et al., 2018) and between the datasets presented in this paper .

The combined clustering for the aggregated libraries used for MSC identification (**Figure 3D-E**, **S4B-D**) was performed using the Seurat package (v.2.3.4, dims=12, resolution=1) (Butler et al., 2018).

Plots were generated either using Seurat (v.3.1.4) or ggplot2 (v.3.2.1) (Wickham, 2016).

Pseudotime analyses and comparison of the developmental lineages

Differential expression analyses were performed using the identified clusters within each dataset to resolve pseudotemporal trajectories using the *setOrderFilter*, *reduceDimension* and *orderCells* function in Monocle (v.2.12.0) (Trapnell et al., 2014). The minimum spanning tree obtained from cells derived from the untreated or ErbBi embryos was rooted on cluster "*twist1a*$^{+}$ Neural Crest" (**Figure 2F**, **3C** and **3H**).

The integrated pseudotime analysis used for the discovery of the MSCs (**Figure 3F**) was based on the combined clustering (**Figure 3D-E**). The cluster "Other NCC derivatives" was excluded from this analysis because it did not contain pigment cell markers. The top 1000 highly dispersed genes among the untreated embryos dataset were chosen as feature genes to resolve the lineage tree using the *setOrderingFilter*, *reduceDimension*, and *orderCells* functions of Monocle (v.2.12.0). We used the default parameters (except for max_components = 4 and norm_method = log) to generate the 3D trajectory during dimensionality reduction. The same genes were then used to order the cells from the ErbBi-treated embryos and then the combined results were plotted using the *PlotComplexTrajectories* function and highlight missing states (states 7,8,11 that were collectively called "MSCs" and plotted back in the original UMAPs) in the ErbBi-treated dataset. The minimum spanning tree was rooted on the "MIX progenitors" cluster. The transcriptome of the cells belonging to the MSC states from untreated embryos were then compared with the ones from cells of the states composing the pigment lineage ("Axon-associated MIs", "Directly-developing melanoblasts ", "MX lineage" and "Pigment progenitors"). The differential expression analysis was performed using a Bayesian approach with the scDE package (v.1.99.4) and the results were plotted using the ggplot2 package (v.3.2.1) and the pathway analysis was performed using the ClusterProfiler R package (v.3.12.0). The same approach was used for the other differential expression analyses presented.

RNA velocity analyses

RNA velocity analyses were performed with the Velocyto R package (v.0.6) (La Manno et al., 2018) using default parameters.

Tfap2b targets

The Tfap2b (Biotin) ChIP-seq data was retrieved from the Gene Expression Omnibus (GEO) under the accession code GSE125711. The same mapping and peak calling pipeline described by the dataset-linked publication was used, with the setting of FDR < 0.01, fold enrichment > 2 set to define the final Tfap2b binding element region. R Package “ChIPseeker” (v1.26.2) (Yu et al., 2015) was used to map the peak coordinates to the gene symbols using chicken genome assembly galGal5. Package “homologene” (v1.5.68.21.2.14) was used to identify human homologous for the gene targets identified in Tfap2b (Biotin) ChIP-seq, as well as the differential expressed genes in the zebrafish cluster (with human homolog *ZEB2* manually mapped to zebrafish gene *zeb2a* as we found it was not automatically mapped by the software).

Other statistical analyses

Counts of dorsal melanocytes in the head and trunk region were performed using the Cell Counter plugin on ImageJ Fiji.

The niche occupancy was calculated as the percentage of GFP+ positive cells per number of visible DRG (**Figure 1**) or as the number of fluorescent cells ventrally to the neural tube (**Figure 5**). Two images per embryos were acquired (caudally to the first somite, ~8 somites; rostrally to the urogenital opening, ~8 somites) and the total number of the niches per embryo were considered.

Statistics for regeneration assays and niche occupancy were performed using running R (v.3.6.2) from RStudio (v.2). For all assays, a normal distribution and equal variance were assumed. For

assays with more than two groups, data was analysed through Analysis of variance (ANOVA), using Tukey-HSD (Honestly Significant Difference) test. Box plots: boxes represent 25^{th} to 75^{th} percentiles, lines are plotted at median. Whiskers represent Min to Max.

SUPPLEMENTAL INFORMATION

Supplementary Figure Legends

Figure S1. Experimental design, analysis pipeline, and quality check results for scRNA-seq experiments.

A. General schematic of the experimental protocol. Collected embryos were separated into two equally sized batches, and one half reared in standard E3 and the other half treated with 5μM AG1478 (ErbB inhibitor, ErbBi) between 6 and 24hpf. Single cell suspensions were generated from each batch of embryos and only $DAPI^-$, GFP^+ and/or $mCherry^+$ were collected and processed with the 10x Genomics Chromium system.

B. Representative FACS plots of the sorted populations.

C. Summary of the analysis pipeline followed.

D - F. Bar plots showing the relation to the Log_{10} library size (**D**), the number of expressed genes (**E**), and the percentage of mitochondrial genes (**F**) of the aggregated libraries from cells pre-quality check (QC).

G - H. Scatter plots distribution of the total features (genes) expressed in relation to the Log_{10} total counts (**G**) and the percentage of mitochondrial genes in relation Log_{10} total counts (**H**) of the aggregated libraries from embryos pre-QC. Red dashed lines indicate the QC thresholds (Total features by counts > 700; Log_{10} total counts > 3.0; Percentage of mitochondrial genes <10%). Gray areas highlight the cells that were considered low quality and excluded from downstream analyses. Orange: cells from untreated embryos, Blue: cells from ErbBi-treated embryos.

I. Principal component analysis (PCA) of the aggregated libraries from cells post-QC. Orange: cells from untreated embryos, Blue: cells from ErbBi-treated embryos.

J. Pie chart of the proportion of cells in a predicted cell cycle phase within the aggregated libraries from cells post-QC.

Figure S2. Proportion of expressed genes and comparison with known datasets.

A, B. Distribution of the Unique Molecular Identifiers (UMIs, **A**) and the expressed genes (**B**) in each cell of the dataset in the different clusters.

C. UMAP of GFP+/DAPI-, mCherry+/DAPI-, and GFP+/mCherry+/DAPI- cells (n = 996 cells) obtained from untreated 24hpf zebrafish embryos after Louvain clustering (dims= 20, resolution = 0.5) showing 6 clusters. The original clusters identifiers are indicated.

D. SanKey plot and UMAP representation based on the scMap results obtained by comparison of the untreated dataset and the Farnsworth et al., 24 hpf dataset.

E. SanKey plot and UMAP representation based on the scMap results obtained by comparison of the untreated dataset and the Wagner et al., 24 hpf dataset.

F. SanKey plot and UMAP representation based on the scMap results obtained by comparison with the Saunders et al., *sox10:CRE*$^{+}$ 5 dpf zebrafish embryos dataset.

Figure S3. mRNA splicing of lineage markers are predictive of cell state progression.

A. Simplified representation of the RNA velocity analysis (**Figure 2B**) with highlighted inferred progression of the cellular state based on the expression of *tfec* (**B**) and the balance between unspliced and spliced mRNAs (**C**).

B. UMAP representation of **Figure 2B** with color change from grey (negative) to red (positive) based on $\log_2$ mRNA expression of *tfec*. *tfec* is expressed in subset of MIX progenitors and is required for the specification of the iridophore lineage (Petratou et al., 2021), suggesting that these will become specified as iridophores whereas the remaining cells within the cluster are MI progenitors. The dashed line around the iridophore state indicates that the state is just inferred. I: Iridophore; M: melanoblast state; MI: melano-iridophore state; MX: melano-xanthophore state.

C. UMAP representations of **Figure 2B** with color change from blue (negative) to red (positive) based on the balance between unspliced and splice mRNAs for *aox5*, *gch2*. Read counts were pooled across the five nearest cell neighbors. The high degradation levels of *aox5* together with positive ratio between unspliced and spliced transcripts for *mitfa* and *gch2* indicate that the MX progenitors are not yet lineage specified and they are most likely the MX progenitors described by Singh and colleagues (Nusslein-Volhard and Singh, 2017; Singh et al., 2016) in the ventro-medial pathway that give rise to melanocytes and a small number of xanthophores

D. Positive ratios of *mitfa* and *tyrp1b* transcripts indicate that cells in the M cluster will likely differentiate into melanoblasts.

Figure S4. ErbB-kinase supports melanocyte lineage differentiation.

A. Heatmap showing the average log_2-fold change expression of five selected genes per cluster identified in **Figure 3B**.

B. Bar plot representing the differences in the proportions of cells within each cluster from untreated and ErbBi-treated embryos. Cells derived from ErbBi-treated and untreated embryos contribute differently to most of the clusters: Other NCC derivatives, p-value = 0.04153; "*twist1a*$^+$ Neural Crest", p-value < 2.2e-16; "Early melanoblasts", p-value = 2.195e^{-6}; MX progenitors, p-value = 9.123e^{-5}; MI progenitor, p-value <2.2e^{-16}; Melanoblasts, p-value = 4.988e^{-10}). The proportions of cells in the *foxd3*$^+$ Neural Crest (p-value=1) and the MIX progenitors (p-value = 0.9342) clusters are not statistically different. 2-sample test for equality of proportions with continuity correction (Z-score test).

C. UMAP representations of **Figures 3D** and **3E** with color change from grey (negative) to blue (positive) based on log_2 mRNA expression of *mitfa, pcna and twist1a*. Cells derived from ErbBi-treated embryos in the "Early melanoblasts" cluster (green dashed line) express genes which are expressed by melanoblasts and *twist1a*$^+$ Neural Crest (blue dashed line).

D. RNA velocity analysis reported on the UMAPs represented in **Figure 3D** (left panel) and **Figure 3E** (right panel). M: melanoblasts; MI: melano-iridophore state; MX: melano-xanthophore state.

Figure S5. *tfap2b* expression in development and melanoma residual disease.

A. *tfap2b* expression in a cluster of cells from melanoma residual disease. Left: UMAP of cells retrieved from GSE136900 (Travnickova et al., 2019) pseudocolored with cell-origin. Right: The same UMAP with color change based on $\log_2$ mRNA expression of *tfap2b*. *tfap2b* is expressed only in Cluster 3 composed of cells derived from the regressed melanomas.

B. Dot-plot representing the average expression of *tfap2b* across lineages identified by integrated pseudotime analysis (**Figure 3C**).

C. Dot-plots representing the average expression of *tfap2b*, *mitfa*, *sox10* and *crestin* in untreated and ErbBi-treated embryo datasets, and in published datasets (Farnsworth et al., 2020; Saunders et al., 2019).

Supplementary tables

Table S1: Metrics, clustering information, and cell states for all cells.

Table S2: Cluster markers.

Table S3: Differential expression analysis of MSCs vs pigment lineage.

Table S4: Pathway analysis of DE genes from MSCs vs pigment lineage.

Table S5: Differential expression analysis of MSCs vs Early pigment progenitors.

Table S6: List of Tfap2b targets.

Table S7: Differential expression analysis of untreated versus ErbBi treated MIX progenitors.

REFERENCES

Adameyko, I., Lallemend, F., Aquino, J.B., Pereira, J.A., Topilko, P., Muller, T., Fritz, N., Beljajeva, A., Mochii, M., Liste, I.*, et al.* (2009). Schwann cell precursors from nerve innervation are a cellular origin of melanocytes in skin. Cell *139*, 366-379.

Bagnara, J.T., Matsumoto, J., Ferris, W., Frost, S.K., Turner, W.A., Jr., Tchen, T.T., and Taylor, J.D. (1979). Common origin of pigment cells. Science *203*, 410-415.

Baxter, L.L., and Pavan, W.J. (2013). The etiology and molecular genetics of human pigmentation disorders. Wiley Interdiscip Rev Dev Biol *2*, 379-392.

Brombin, A., Joly, J.S., and Jamen, F. (2015). New tricks for an old dog: ribosome biogenesis contributes to stem cell homeostasis. Curr Opin Genet Dev *34*, 61-70.

Budi, E.H., Patterson, L.B., and Parichy, D.M. (2008). Embryonic requirements for ErbB signaling in neural crest development and adult pigment pattern formation. Development *135*, 2603-2614.

Budi, E.H., Patterson, L.B., and Parichy, D.M. (2011). Post-embryonic nerve-associated precursors to adult pigment cells: genetic requirements and dynamics of morphogenesis and differentiation. PLoS Genet *7*, e1002044.

Butler, A., Hoffman, P., Smibert, P., Papalexi, E., and Satija, R. (2018). Integrating single-cell transcriptomic data across different conditions, technologies, and species. Nat Biotechnol *36*, 411-420.

Camargo-Sosa, K., Colanesi, S., Muller, J., Schulte-Merker, S., Stemple, D., Patton, E.E., and Kelsh, R.N. (2019). Endothelin receptor Aa regulates proliferation and differentiation of Erb-dependent pigment progenitors in zebrafish. PLoS Genet *15*, e1007941.

Chong-Morrison, V., and Sauka-Spengler, T. (2021). The Cranial Neural Crest in a Multiomics Era. Front Physiol *12*, 634440.

Diener, J., and Sommer, L. (2020). Reemergence of neural crest stem cell-like states in melanoma during disease progression and treatment. Stem Cells Transl Med.

Dooley, C.M., Mongera, A., Walderich, B., and Nusslein-Volhard, C. (2013). On the embryonic origin of adult melanophores: the role of ErbB and Kit signalling in establishing melanophore stem cells in zebrafish. Development *140*, 1003-1013.

Ernfors, P. (2010). Cellular origin and developmental mechanisms during the formation of skin melanocytes. Exp Cell Res *316*, 1397-1407.

Farnsworth, D.R., Saunders, L.M., and Miller, A.C. (2020). A single-cell transcriptome atlas for zebrafish development. Dev Biol *459*, 100-108.

Furlan, A., and Adameyko, I. (2018). Schwann cell precursor: a neural crest cell in disguise? Dev Biol *444 Suppl 1*, S25-s35.

Gabut, M., Bourdelais, F., and Durand, S. (2020). Ribosome and Translational Control in Stem Cells. Cells *9*.

Gupta, S., and Santoro, R. (2020). Regulation and Roles of the Nucleolus in Embryonic Stem Cells: From Ribosome Biogenesis to Genome Organization. Stem Cell Reports *15*, 1206-1219.

Hultman, K.A., Budi, E.H., Teasley, D.C., Gottlieb, A.Y., Parichy, D.M., and Johnson, S.L. (2009). Defects in ErbB-dependent establishment of adult melanocyte stem cells reveal independent origins for embryonic and regeneration melanocytes. PLoS Genet *5*, e1000544.

Hultman, K.A., and Johnson, S.L. (2010). Differential contribution of direct-developing and stem cell-derived melanocytes to the zebrafish larval pigment pattern. Dev Biol *337*, 425-431.

Irion, U., and Nusslein-Volhard, C. (2019). The identification of genes involved in the evolution of color patterns in fish. Curr Opin Genet Dev *57*, 31-38.

Irion, U., Singh, A.P., and Nusslein-Volhard, C. (2016). The Developmental Genetics of Vertebrate Color Pattern Formation: Lessons from Zebrafish. Curr Top Dev Biol *117*, 141-169.

Johansson, J.A., Marie, K.L., Lu, Y., Brombin, A., Santoriello, C., Zeng, Z., Zich, J., Gautier, P., von Kriegsheim, A., Brunsdon, H.*, et al.* (2020). PRL3-DDX21 Transcriptional Control of Endolysosomal Genes Restricts Melanocyte Stem Cell Differentiation. Dev Cell *54*, 317-332 e319.

Johnson, S.L., Nguyen, A.N., and Lister, J.A. (2011). mitfa is required at multiple stages of melanocyte differentiation but not to establish the melanocyte stem cell. Dev Biol *350*, 405-413.

Kaufman, C.K., Mosimann, C., Fan, Z.P., Yang, S., Thomas, A.J., Ablain, J., Tan, J.L., Fogley, R.D., van Rooijen, E., Hagedorn, E.J.*, et al.* (2016). A zebrafish melanoma model reveals emergence of neural crest identity during melanoma initiation. Science *351*, aad2197.

Kelsh, R.N., and Barsh, G.S. (2011). A nervous origin for fish stripes. PLoS Genet *7*, e1002081.

Kelsh, R.N., Brand, M., Jiang, Y.J., Heisenberg, C.P., Lin, S., Haffter, P., Odenthal, J., Mullins, M.C., van Eeden, F.J., Furutani-Seiki, M.*, et al.* (1996). Zebrafish pigmentation mutations and the processes of neural crest development. Development *123*, 369-389.

Kharchenko, P.V., Silberstein, L., and Scadden, D.T. (2014). Bayesian approach to single-cell differential expression analysis. Nature Methods *11*, 740-742.

Kimmel, C.B., Ballard, W.W., Kimmel, S.R., Ullmann, B., and Schilling, T.F. (1995). Stages of embryonic development of the zebrafish. Dev Dyn *203*, 253-310.

Kinsler, V.A., and Larue, L. (2018). The patterns of birthmarks suggest a novel population of melanocyte precursors arising around the time of gastrulation. Pigment Cell Melanoma Res *31*, 95-109.

Kiselev, V.Y., Yiu, A., and Hemberg, M. (2018). scmap: projection of single-cell RNA-seq data across data sets. Nat Methods *15*, 359-362.

Knight, R.D., Javidan, Y., Zhang, T., Nelson, S., and Schilling, T.F. (2005). AP2-dependent signals from the ectoderm regulate craniofacial development in the zebrafish embryo. Development *132*, 3127-3138.

Konieczkowski, D.J., Johannessen, C.M., Abudayyeh, O., Kim, J.W., Cooper, Z.A., Piris, A., Frederick, D.T., Barzily-Rokni, M., Straussman, R., Haq, R.*, et al.* (2014). A melanoma cell state distinction influences sensitivity to MAPK pathway inhibitors. Cancer Discov *4*, 816-827.

Krauss, J., Geiger-Rudolph, S., Koch, I., Nusslein-Volhard, C., and Irion, U. (2014). A dominant mutation in tyrp1A leads to melanophore death in zebrafish. Pigment Cell Melanoma Res *27*, 827-830.

Kwan, K.M., Fujimoto, E., Grabher, C., Mangum, B.D., Hardy, M.E., Campbell, D.S., Parant, J.M., Yost, H.J., Kanki, J.P., and Chien, C.B. (2007). The Tol2kit: a multisite gateway-based construction kit for Tol2 transposon transgenesis constructs. Dev Dyn *236*, 3088-3099.

La Manno, G., Soldatov, R., Zeisel, A., Braun, E., Hochgerner, H., Petukhov, V., Lidschreiber, K., Kastriti, M.E., Lonnerberg, P., Furlan, A.*, et al.* (2018). RNA velocity of single cells. Nature *560*, 494-498.

Lee, J.H., and Fisher, D.E. (2014). Melanocyte stem cells as potential therapeutics in skin disorders. Expert Opin Biol Ther *14*, 1569-1579.

Li, L., Fukunaga-Kalabis, M., Yu, H., Xu, X., Kong, J., Lee, J.T., and Herlyn, M. (2010). Human dermal stem cells differentiate into functional epidermal melanocytes. J Cell Sci *123*, 853-860.

Lignell, A., Kerosuo, L., Streichan, S.J., Cai, L., and Bronner, M.E. (2017). Identification of a neural crest stem cell niche by Spatial Genomic Analysis. Nat Commun *8*, 1830.

Ling, I.T.C., and Sauka-Spengler, T. (2019). Early chromatin shaping predetermines multipotent vagal neural crest into neural, neuronal and mesenchymal lineages. Nature Cell Biology *21*, 1504-1517.

Lun, A.T., McCarthy, D.J., and Marioni, J.C. (2016). A step-by-step workflow for low-level analysis of single-cell RNA-seq data with Bioconductor. F1000Res *5*, 2122.

Manoli, M., and Driever, W. (2012). Fluorescence-activated cell sorting (FACS) of fluorescently tagged cells from zebrafish larvae for RNA isolation. Cold Spring Harb Protoc *2012*.

Marie, K.L., Sassano, A., Yang, H.H., Michalowski, A.M., Michael, H.T., Guo, T., Tsai, Y.C., Weissman, A.M., Lee, M.P., Jenkins, L.M., *et al.* (2020). Melanoblast transcriptome analysis reveals pathways promoting melanoma metastasis. Nat Commun *11*, 333.

Marine, J.C., Dawson, S.J., and Dawson, M.A. (2020). Non-genetic mechanisms of therapeutic resistance in cancer. Nat Rev Cancer *20*, 743-756.

McCarthy, D.J., Campbell, K.R., Lun, A.T., and Wills, Q.F. (2017). Scater: pre-processing, quality control, normalization and visualization of single-cell RNA-seq data in R. Bioinformatics *33*, 1179-1186.

McInnes, L., Healy, J., and Melville, J. (2018). UMAP: Uniform Manifold Approximation and Projection for Dimension Reduction, pp. arXiv:1802.03426.

Moon, H., Donahue, L.R., Choi, E., Scumpia, P.O., Lowry, W.E., Grenier, J.K., Zhu, J., and White, A.C. (2017). Melanocyte Stem Cell Activation and Translocation Initiate Cutaneous Melanoma in Response to UV Exposure. Cell Stem Cell *21*, 665-678 e666.

Mort, R.L., Jackson, I.J., and Patton, E.E. (2015). The melanocyte lineage in development and disease. Development *142*, 620-632.

Mosimann, C., Kaufman, C.K., Li, P., Pugach, E.K., Tamplin, O.J., and Zon, L.I. (2011). Ubiquitous transgene expression and Cre-based recombination driven by the ubiquitin promoter in zebrafish. Development *138*, 169-177.

Nestorowa, S., Hamey, F.K., Pijuan Sala, B., Diamanti, E., Shepherd, M., Laurenti, E., Wilson, N.K., Kent, D.G., and Gottgens, B. (2016). A single-cell resolution map of mouse hematopoietic stem and progenitor cell differentiation. Blood *128*, e20-31.

Nusslein-Volhard, C., and Singh, A.P. (2017). How fish color their skin: A paradigm for development and evolution of adult patterns: Multipotency, plasticity, and cell competition regulate proliferation and spreading of pigment cells in Zebrafish coloration. Bioessays *39*.

O'Reilly-Pol, T., and Johnson, S.L. (2009). Melanocyte regeneration reveals mechanisms of adult stem cell regulation. Semin Cell Dev Biol *20*, 117-124.

Okamoto, N., Aoto, T., Uhara, H., Yamazaki, S., Akutsu, H., Umezawa, A., Nakauchi, H., Miyachi, Y., Saida, T., and Nishimura, E.K. (2014). A melanocyte--melanoma precursor niche in sweat glands of volar skin. Pigment Cell Melanoma Res *27*, 1039-1050.

Owen, J.P., Kelsh, R.N., and Yates, C.A. (2020). A quantitative modelling approach to zebrafish pigment pattern formation. Elife *9*.

Parichy, D.M., Elizondo, M.R., Mills, M.G., Gordon, T.N., and Engeszer, R.E. (2009). Normal table of postembryonic zebrafish development: staging by externally visible anatomy of the living fish. Dev Dyn *238*, 2975-3015.

Parichy, D.M., and Spiewak, J.E. (2015). Origins of adult pigmentation: diversity in pigment stem cell lineages and implications for pattern evolution. Pigment Cell Melanoma Res *28*, 31-50.

Patton, E.E., Mueller, K.L., Adams, D.J., Anandasabapathy, N., Aplin, A.E., Bertolotto, C., Bosenberg, M., Ceol, C.J., Burd, C.E., Chi, P.*, et al.* (2021). Melanoma models for the next generation of therapies. Cancer Cell *39*, 610-631.

Petratou, K., Spencer, S.A., Kelsh, R.N., and Lister, J.A. (2021). The MITF paralog tfec is required in neural crest development for fate specification of the iridophore lineage from a multipotent pigment cell progenitor. PLoS One *16*, e0244794.

Petratou, K., Subkhankulova, T., Lister, J.A., Rocco, A., Schwetlick, H., and Kelsh, R.N. (2018). A systems biology approach uncovers the core gene regulatory network governing iridophore fate choice from the neural crest. PLoS Genet *14*, e1007402.

Praetorius, C., Grill, C., Stacey, S.N., Metcalf, A.M., Gorkin, D.U., Robinson, K.C., Van Otterloo, E., Kim, R.S., Bergsteinsdottir, K., Ogmundsdottir, M.H.*, et al.* (2013). A polymorphism in IRF4 affects human pigmentation through a tyrosinase-dependent MITF/TFAP2A pathway. Cell *155*, 1022-1033.

Qiu, X., Mao, Q., Tang, Y., Wang, L., Chawla, R., Pliner, H.A., and Trapnell, C. (2017). Reversed graph embedding resolves complex single-cell trajectories. Nat Methods *14*, 979-982.

Rambow, F., Rogiers, A., Marin-Bejar, O., Aibar, S., Femel, J., Dewaele, M., Karras, P., Brown, D., Chang, Y.H., Debiec-Rychter, M.*, et al.* (2018). Toward Minimal Residual Disease-Directed Therapy in Melanoma. Cell *174*, 843-855 e819.

Recher, G., Jouralet, J., Brombin, A., Heuze, A., Mugniery, E., Hermel, J.M., Desnoulez, S., Savy, T., Herbomel, P., Bourrat, F.*, et al.* (2013). Zebrafish midbrain slow-amplifying progenitors exhibit high levels of transcripts for nucleotide and ribosome biogenesis. Development *140*, 4860-4869.

Rothstein, M., and Simoes-Costa, M. (2020). Heterodimerization of TFAP2 pioneer factors drives epigenomic remodeling during neural crest specification. Genome Res *30*, 35-48.

Saunders, L.M., Mishra, A.K., Aman, A.J., Lewis, V.M., Toomey, M.B., Packer, J.S., Qiu, X., McFaline-Figueroa, J.L., Corbo, J.C., Trapnell, C.*, et al.* (2019). Thyroid hormone regulates distinct paths to maturation in pigment cell lineages. Elife *8*.

Seberg, H.E., Van Otterloo, E., Loftus, S.K., Liu, H., Bonde, G., Sompallae, R., Gildea, D.E., Santana, J.F., Manak, J.R., Pavan, W.J.*, et al.* (2017). TFAP2 paralogs regulate melanocyte differentiation in parallel with MITF. PLoS Genet *13*, e1006636.

Shakhova, O., Zingg, D., Schaefer, S.M., Hari, L., Civenni, G., Blunschi, J., Claudinot, S., Okoniewski, M., Beermann, F., Mihic-Probst, D.*, et al.* (2012). Sox10 promotes the formation and maintenance of giant congenital naevi and melanoma. Nat Cell Biol *14*, 882-890.

Shen, S., Vagner, S., and Robert, C. (2020). Persistent Cancer Cells: The Deadly Survivors. Cell *183*, 860-874.

Singh, A.P., Dinwiddie, A., Mahalwar, P., Schach, U., Linker, C., Irion, U., and Nusslein-Volhard, C. (2016). Pigment Cell Progenitors in Zebrafish Remain Multipotent through Metamorphosis. Dev Cell *38*, 316-330.

Singh, A.P., Schach, U., and Nusslein-Volhard, C. (2014). Proliferation, dispersal and patterned aggregation of iridophores in the skin prefigure striped colouration of zebrafish. Nat Cell Biol *16*, 607-614.

Stuart, T., Butler, A., Hoffman, P., Hafemeister, C., Papalexi, E., Mauck, W.M., III, Hao, Y., Stoeckius, M., Smibert, P., and Satija, R. (2019). Comprehensive Integration of Single-Cell Data. Cell *177*, 1888-1902.e1821.

Sun, Q., Lee, W., Mohri, Y., Takeo, M., Lim, C.H., Xu, X., Myung, P., Atit, R.P., Taketo, M.M., Moubarak, R.S*., et al.* (2019). A novel mouse model demonstrates that oncogenic melanocyte stem cells engender melanoma resembling human disease. Nat Commun *10*, 5023.

Taylor, K.L., Lister, J.A., Zeng, Z., Ishizaki, H., Anderson, C., Kelsh, R.N., Jackson, I.J., and Patton, E.E. (2011). Differentiated melanocyte cell division occurs in vivo and is promoted by mutations in Mitf. Development *138*, 3579-3589.

Trapnell, C., Cacchiarelli, D., Grimsby, J., Pokharel, P., Li, S., Morse, M., Lennon, N.J., Livak, K.J., Mikkelsen, T.S., and Rinn, J.L. (2014). The dynamics and regulators of cell fate decisions are revealed by pseudotemporal ordering of single cells. Nat Biotechnol *32*, 381-386.

Travnickova, J., and Patton, E.E. (2021). Deciphering Melanoma Cell States and Plasticity with Zebrafish Models. J Invest Dermatol *141*, 1389-1394.

Travnickova, J., Wojciechowska, S., Khamseh, A., Gautier, P., Brown, D.V., Lefevre, T., Brombin, A., Ewing, A., Capper, A., Spitzer, M*., et al.* (2019). Zebrafish MITF-Low Melanoma Subtype Models Reveal Transcriptional Subclusters and MITF-Independent Residual Disease. Cancer Res *79*, 5769-5784.

Tryon, R.C., Higdon, C.W., and Johnson, S.L. (2011). Lineage relationship of direct-developing melanocytes and melanocyte stem cells in the zebrafish. PLoS One *6*, e21010.

Varum, S., Baggiolini, A., Zurkirchen, L., Atak, Z.K., Cantu, C., Marzorati, E., Bossart, R., Wouters, J., Hausel, J., Tuncer, E*., et al.* (2019). Yin Yang 1 Orchestrates a Metabolic Program Required for Both Neural Crest Development and Melanoma Formation. Cell Stem Cell *24*, 637-653 e639.

Wagner, D.E., Weinreb, C., Collins, Z.M., Briggs, J.A., Megason, S.G., and Klein, A.M. (2018). Single-cell mapping of gene expression landscapes and lineage in the zebrafish embryo. Science *360*, 981-987.

White, R.M., Cech, J., Ratanasirintrawoot, S., Lin, C.Y., Rahl, P.B., Burke, C.J., Langdon, E., Tomlinson, M.L., Mosher, J., Kaufman, C.*, et al.* (2011). DHODH modulates transcriptional elongation in the neural crest and melanoma. Nature *471*, 518-522.

Wickham, H. (2016). ggplot2: Elegant Graphics for Data Analysis (Springer-Verlag New York).

Yu, G., Wang, L.G., Han, Y., and He, Q.Y. (2012). clusterProfiler: an R package for comparing biological themes among gene clusters. OMICS *16*, 284-287.

Yu, G., Wang, L.G., and He, Q.Y. (2015). ChIPseeker: an R/Bioconductor package for ChIP peak annotation, comparison and visualization. Bioinformatics *31*, 2382-2383.

Zabierowski, S.E., Fukunaga-Kalabis, M., Li, L., and Herlyn, M. (2011). Dermis-derived stem cells: a source of epidermal melanocytes and melanoma? Pigment Cell Melanoma Res *24*, 422-429.

Zeng, Z., Johnson, S.L., Lister, J.A., and Patton, E.E. (2015). Temperature-sensitive splicing of mitfa by an intron mutation in zebrafish. Pigment Cell Melanoma Res *28*, 229-232.

Zhou, L., Ishizaki, H., Spitzer, M., Taylor, K.L., Temperley, N.D., Johnson, S.L., Brear, P., Gautier, P., Zeng, Z., Mitchell, A.*, et al.* (2012). ALDH2 mediates 5-nitrofuran activity in multiple species. Chem Biol *19*, 883-892.

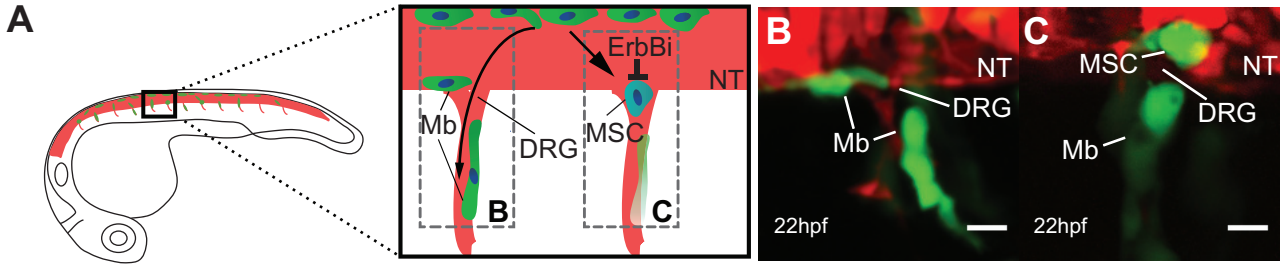

Tg (mitfa:GFP; nbt:dsRed)

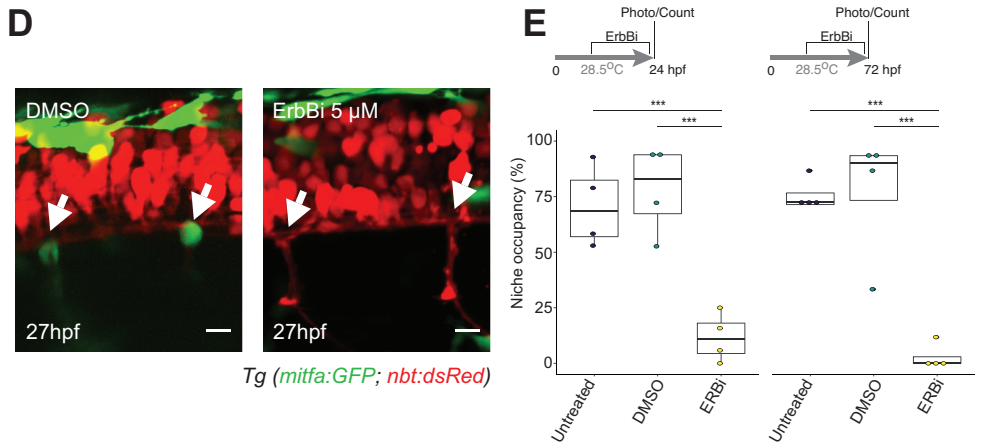

Tg (crestin:mCherry; mitfa:GFP)

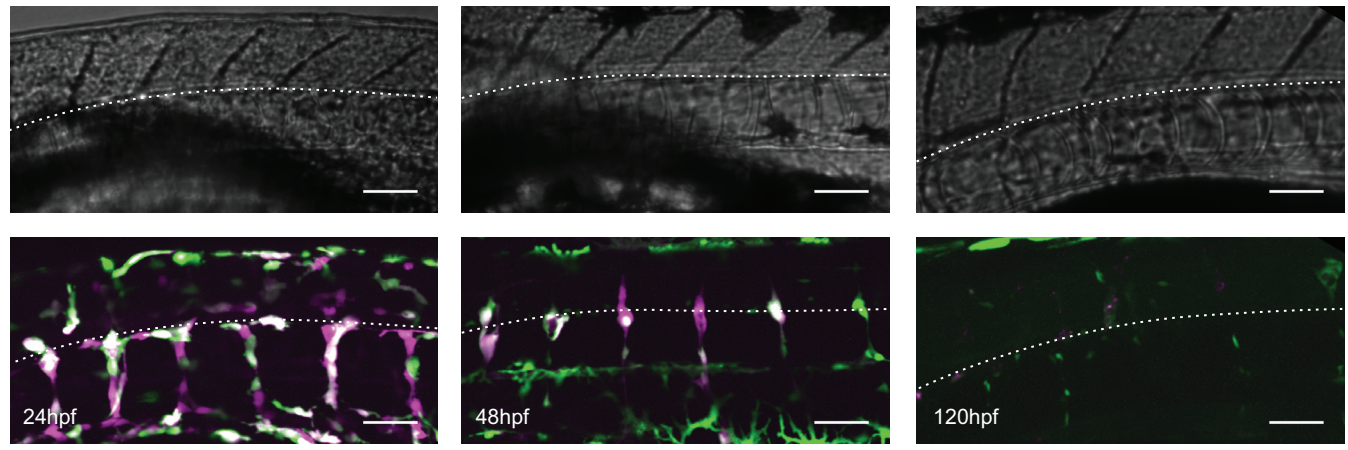

Tg (crestin:mCherry; mitfa:GFP)

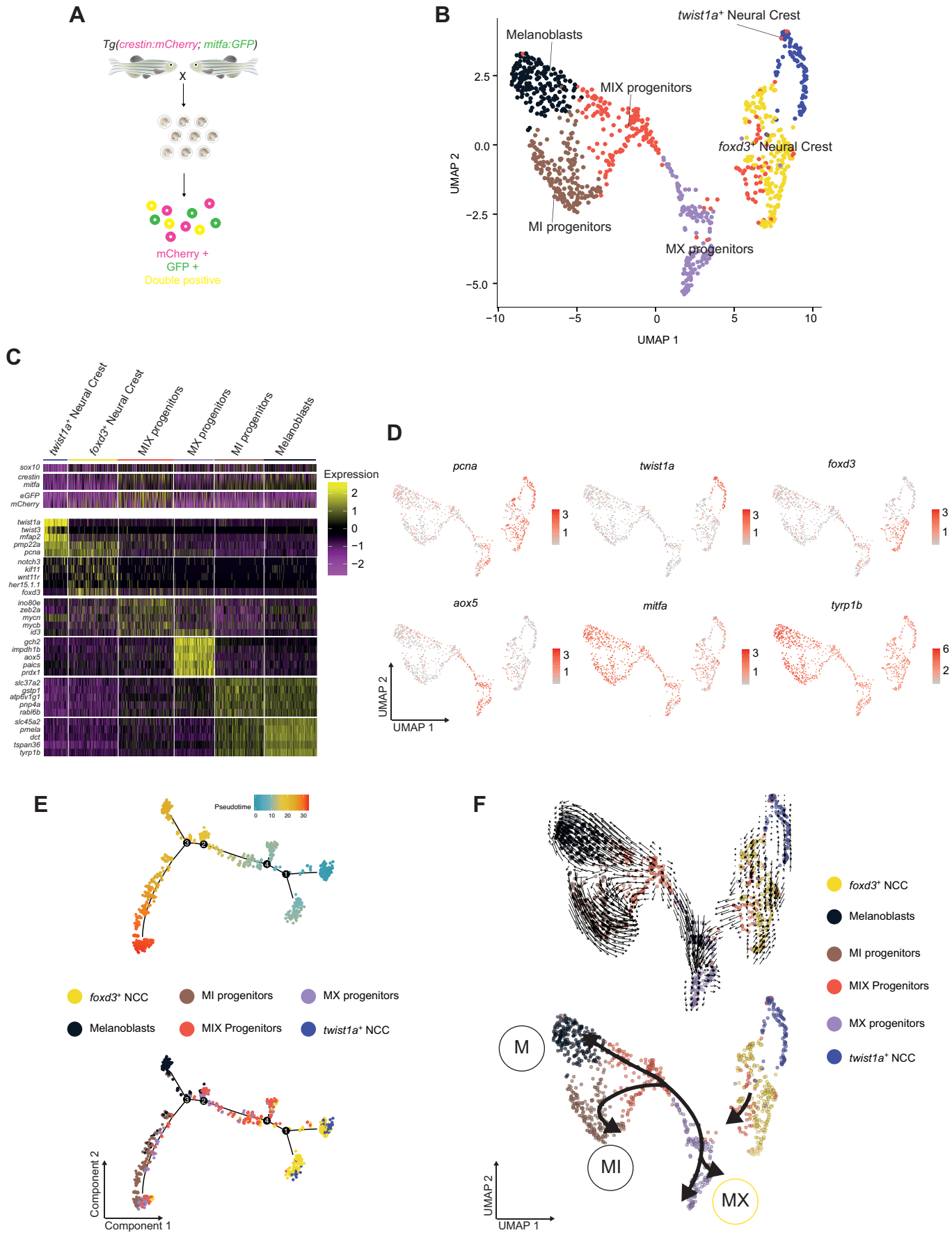

Brombin *et al.*, - Figure 2

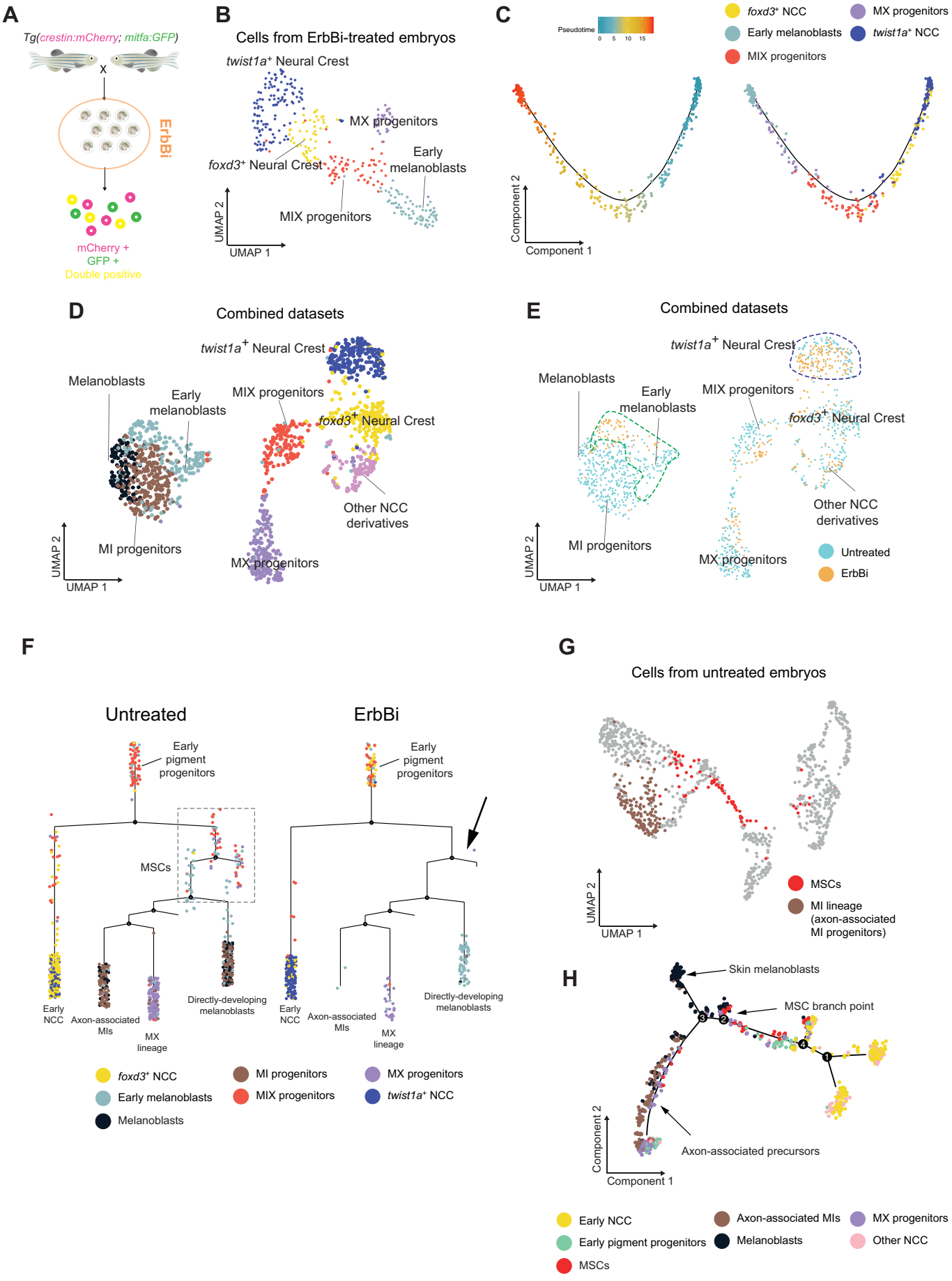

Brombin *et al.*, - Figure 3

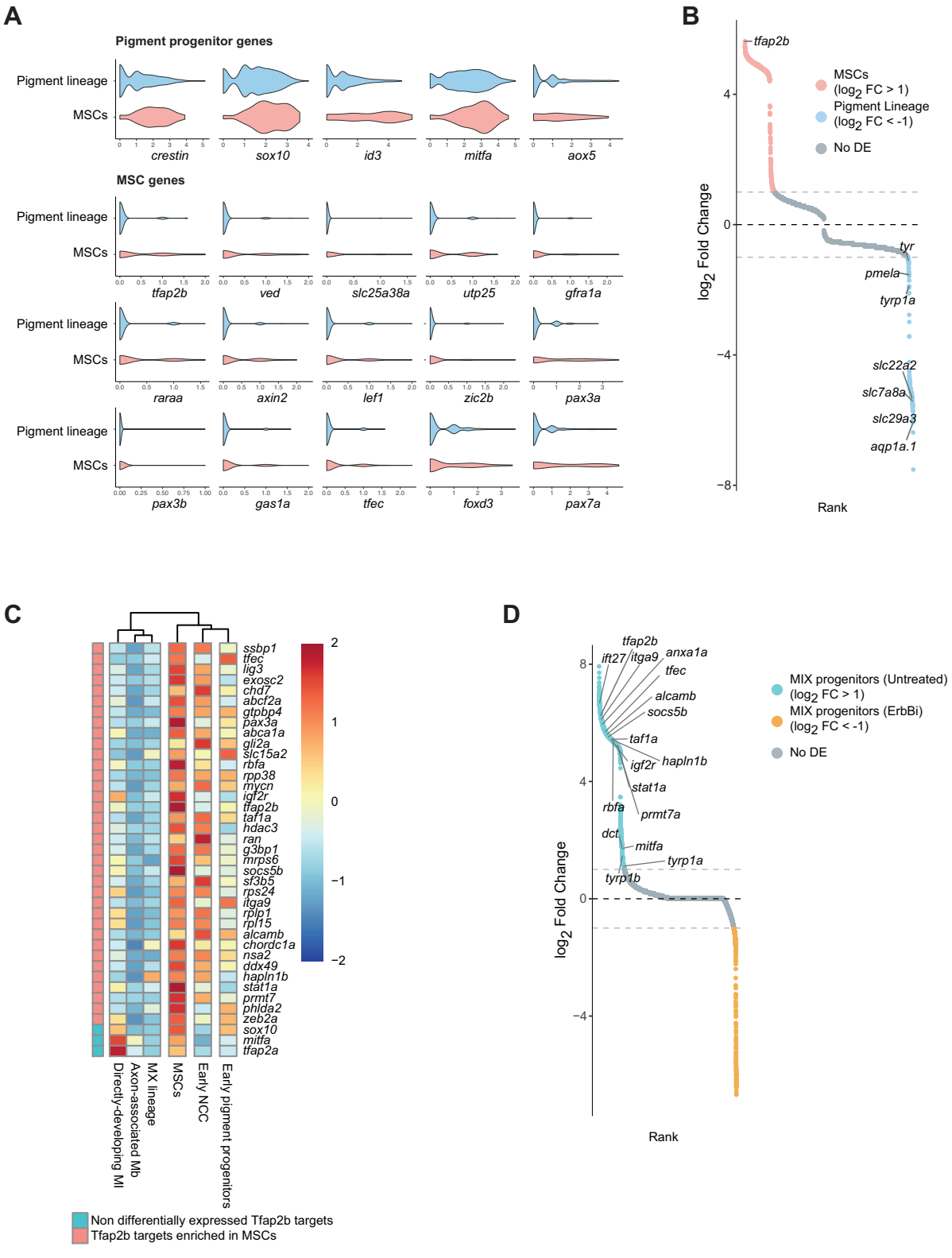

Brombin *et al.*, - Figure 4

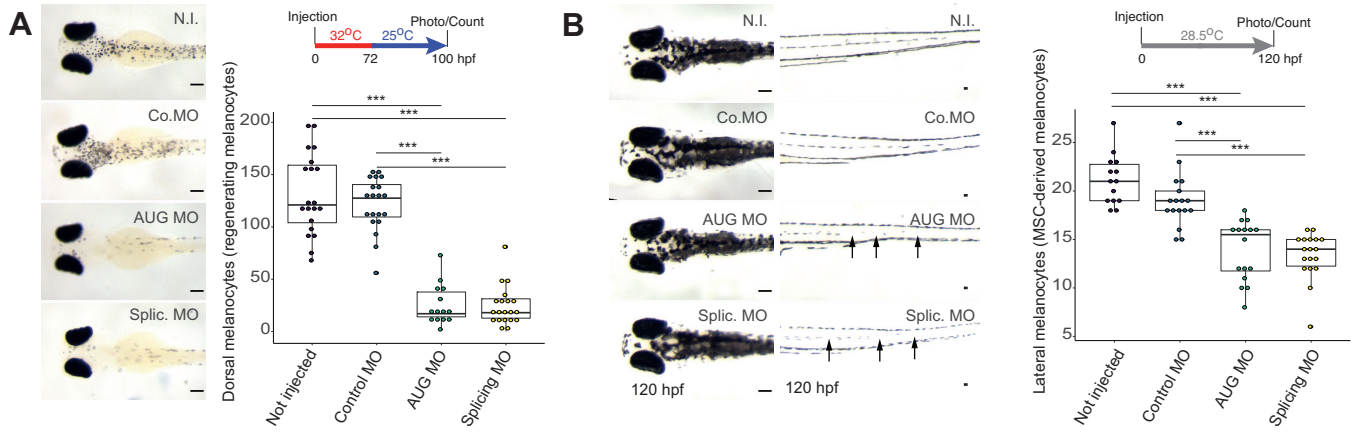

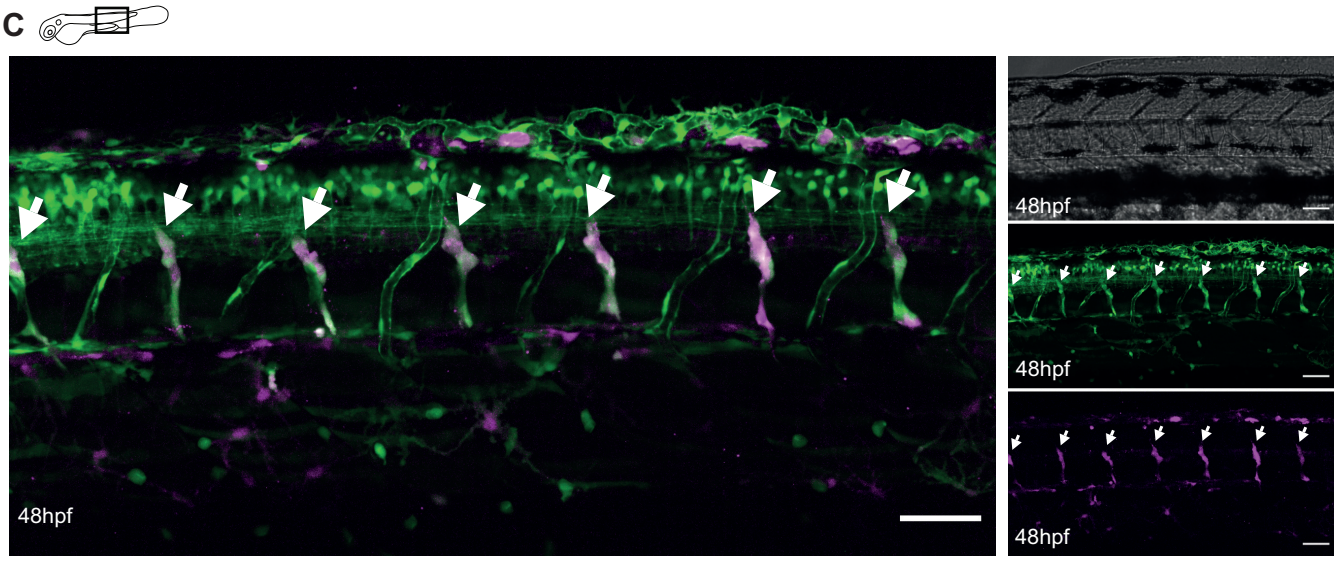

Tg (crestin:mCherry; tfap2b:eGFP)

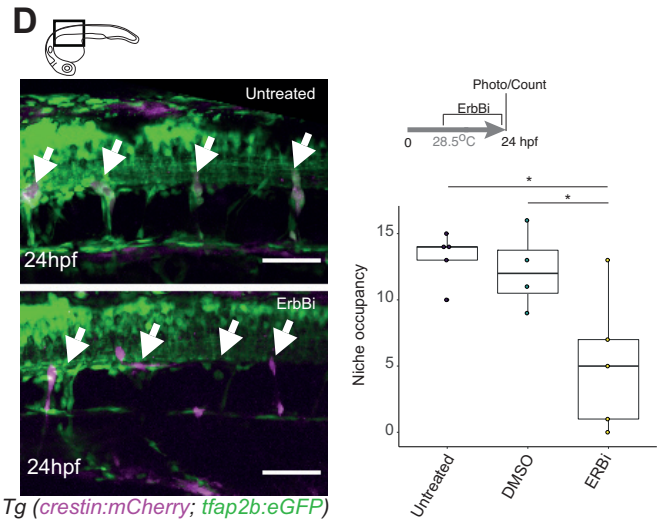

Tg (crestin:mCherry; tfap2b:eGFP)

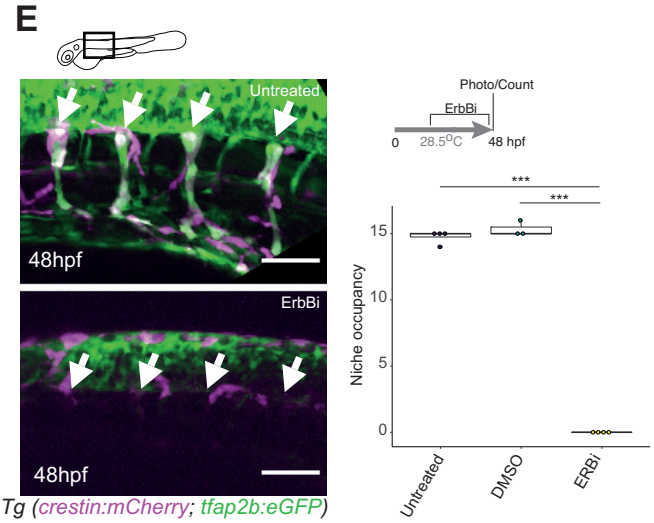

Tg (crestin:mCherry; tfap2b:eGFP)

Brombin *et al.*, - Figure 5

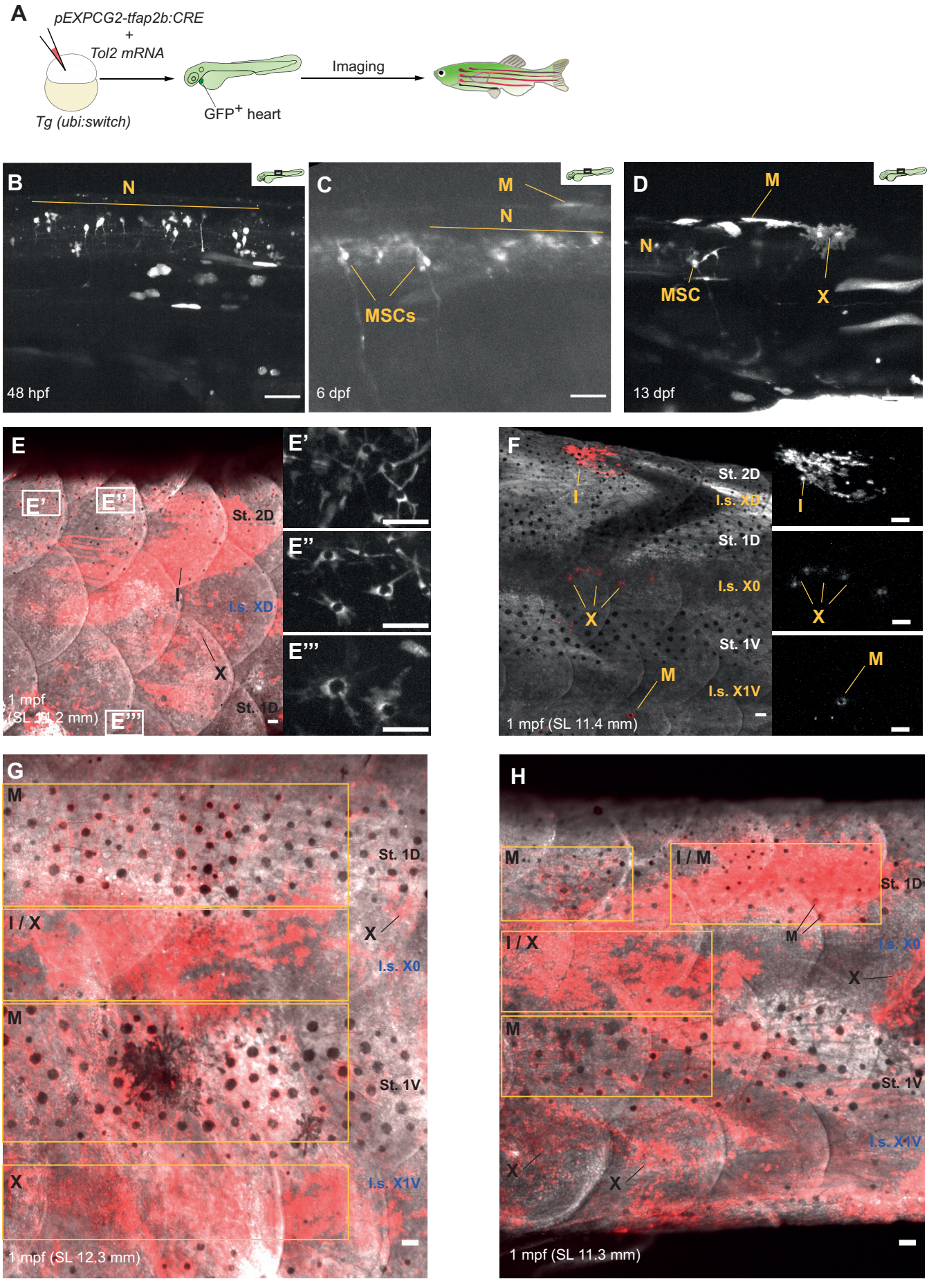

Brombin *et al.*, - Figure 6